Journal of Medicinal Chemistry

Article

#-Secretase (BACE1) Inhibitors with High In Vivo Efficacy Suitable for Clinical Evaluation in Alzheimer's Disease

Hans Hilpert, Wolfgang Guba, Thomas J. Woltering, Wolfgang Wostl, Emmanuel Pinard, Harald Mauser, Alexander V Mayweg, Mark Rogers-Evans, Roland Humm, Daniela Krummenacher, Thorsten Muser, Christian Schnider, Helmut Jacobsen, Laurence Ozmen, Alessandra Bergadano, David W. Banner, Remo Hochstrasser, Andreas Kuglstatter, Pascale David-Pierson, Holger Fischer, Alessandra Polara, and Robert Narquizian

J. Med. Chem., **Just Accepted Manuscript** • DOI: 10.1021/jm400225m • Publication Date (Web): 16 Apr 2013

β-Secretase (BACE1) Inhibitors with High *In Vivo* Efficacy Suitable for Clinical Evaluation in Alzheimer's Disease

Hans Hilpert,*[,†] Wolfgang Guba,[†] Thomas J. Woltering,[†] Wolfgang Wostl,[†] Emmanuel Pinard,[†] Harald Mauser,[†] Alexander V. Mayweg,[†] Mark Rogers-Evans,[†] Roland Humm,[†] Daniela Krummenacher,[†] Thorsten Muser,[†] Christian Schnider,[†] Helmut Jacobsen,[‡] Laurence Ozmen,[‡] Alessandra Bergadano,[‡] David W. Banner,[§] Remo Hochstrasser,[§] Andreas Kuglstatter,[§] Pascale David-Pierson,[#] Holger Fischer,[#] Alessandra Polara,[∥] Robert Narquizian[∥]

[†]Discovery Chemistry, [‡]DTA Neuroscience, [§]Discovery Technologies, [#]Drug Metabolism and Pharmacokinetics, [∥]Roche Partnering, F. Hoffmann-La Roche Ltd, pRED, Pharma Research & Early Development, Grenzacherstrasse 124, Basel, Switzerland, CH-4070

ABSTRACT: An extensive fluorine scan of 1,3-oxazines revealed the power of fluorine(s) to lower the pKa and thereby dramatically change the pharmacological profile of this class of BACE1 inhibitors. The CF_3 substituted oxazine **89**, a potent and highly brain penetrant BACE1 inhibitor, was able to reduce significantly CSF Aβ40 & 42 in rats at oral doses as low as 1 mg/kg. The effect was long lasting, showing a significant reduction of Aβ40 & 42 even after 24 h. In contrast to **89**, compound **1b** lacking the CF_3 group was virtually inactive *in vivo*.

INTRODUCTION

Alzheimer's disease (AD) is a progressive neurodegenerative disease, and the major cause of dementia in the elderly. The clinical symptoms of AD are progressive memory loss, learning impairment and

behavioral and psychiatric disturbances. The predominant pathological hallmarks of the disease are 1. amyloid plaques, i.e., extracellular deposits of polymerized amyloid-β peptides (Aβ), and 2. intracellular aggregates of mis-folded tau protein. Formation of these pathologies can precede the clinical disease symptoms by years. The final disease pathology is further characterized by pronounced neuroinflammation and widespread neuronal loss. As no causative treatment is currently available, there is an urgent need for new, efficacious therapies.[1] Amyloid aggregates are considered to be the earliest pathology, and according to the amyloid cascade hypothesis, the ultimate cause of the disease.[2-5] Their main constituents, the amyloid-β peptides, are derived from the β-amyloid precursor protein (APP) via proteolytic processing by β-secretase (BACE1) and γ-secretase. Both APP and BACE1 are type-1 membrane proteins highly expressed in the brain. BACE1 is an aspartic protease of 501 amino acids length, organized into an extracellular domain with signal peptide, prodomain and catalytic domain, a transmembrane domain and a short cytoplasmic stretch of 22 amino acids. Its principal cleavage site in the APP extracellular domain forms the N-terminus of Aβ (position D672 of the longest APP isotype); a secondary cleavage site is localized at position E682. Processing of APP occurs predominantly in endosomal vesicles, in agreement with the "acidic pH" optimum" of the enzyme.[6-8] The unique and essential role of BACE1 for the generation of Aβ has been convincingly shown in mice where both alleles have been ablated by genetic means. These mice do not form Aβ, nor do they cleave APP at the known BACE1-positions.[9, 10] It has furthermore been demonstrated that upon crossing BACE1 knock-out mice and APP-transgenic mice, the formation of brain amyloid is inhibited. Interestingly, ablation of only one BACE1 allele was enough to reduce amyloidosis significantly. These data suggest that pharmacological inhibition of BACE1 should also reduce amyloidosis, and that partial inhibition should be sufficient to achieve therapeutic efficacy.[11, 12] Taken together this makes BACE1 a prime target for anti-amyloid therapy. Partial inhibition of BACE1 may also be the preferred therapeutic target, since a number of additional BACE1 substrates have been described. Of special interest is neuregulin 1 (NRG1) processing, since close examination of BACE1 knock-out mice has revealed that in these animals the

myelination of peripheral and possibly central nerves is severely reduced, presumably due to the absence of NRG1 processing.[13, 14] Importantly, this adverse effect was not observed in animals that retained one functional allele.

The aspartyl protease BACE2 is a close homolog of BACE1. BACE2, however, cleaves APP preferentially at a position downstream of the BACE1 cleavage sites at F691 of APP, which does not produce amyloidogenic Aβ peptides. BACE2 is primarily expressed in peripheral tissue, in particular in pancreatic islets.[15] Its physiological function was poorly understood for some time,[8] but recent evidence suggests that it may play a role in glucose homeostasis.[15]

Soon after the discovery of BACE1 in 1999,[16-20] the enzyme became a prime target of both academic and industrial research. Initial inhibitor design focused on statine type structures engaging with the two aspartic acids in the catalytic site. While potent *in vitro*, the peptidic nature of these inhibitors rendered them poorly brain penetrant. To overcome this shortcoming, less peptidic hydroxyethylamine (HEA) isosters subsequently became the focus of research. Good brain penetration, however, remained the exception rather than the rule. This has been ascribed to the flexibility of HEAs and their high number of hydrogen bond donors and acceptors.[21]

Our research focused on cyclic, conformationally rigid structures that interact with the two aspartic acids of BACE1. An HTS campaign yielded a small fragment of a weakly active (IC_{50}=41.2 μM) 2-amino-4H-5,6-dihydro-[1,3]thiazine derivative **A** (Figure 1) which could be co-crystallized with BACE1, offering unique opportunities for optimization. This heterocycle was first synthesized at Roche more than 30 years ago in a project looking for novel analgesics,[22] and has later been explored by various research groups[23-28] as a head group interacting with the aspartic acids of BACE1.

Previously we described the identification and characterization of a number of cyclic amidines that were devoid of substantial *in vivo* activity due to low penetration into the CNS.[29] In this paper we disclose our efforts to convert our initial lead compound, the 2-amino-4H-5,6-dihydro-[1,3]oxazine

derivative **1a** into fluorine containing oxazines **B**, a compound class characterized by high *in vivo* activity and good overall properties.

Figure 1. Lead Compound **1a** and Targeted Fluoro-oxazines **B**.

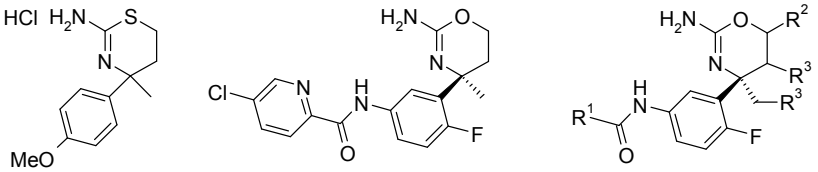

CHEMISTRY

The syntheses of oxazines **1a-b** and difluoro-oxazines **14a-v** (Scheme 1) started with elegant work developed by Ellman.[30] Condensation of the chiral auxiliary (R)-*tert*-butanesulfinamide and acetophenone **2** in the presence of $Ti(OEt)_4$ gave the sulfinyl imine **3**. Transmetalation of the lithium enolate of ethyl acetate using $TiCl(OiPr)_3$ generated the titanium enolate which reacted with the sulfinyl imine **3** to furnish the ester **4** as a single diastereoisomer. Alternatively, the Reformatsky reaction of the sulfinyl imine **3** and ethyl bromodifluoroacetate[31] furnished the α,α-difluoroester **5**.

Scheme 1. Synthesis of Oxazines 1a-b and Difluoro-oxazines 14a-v.[a]

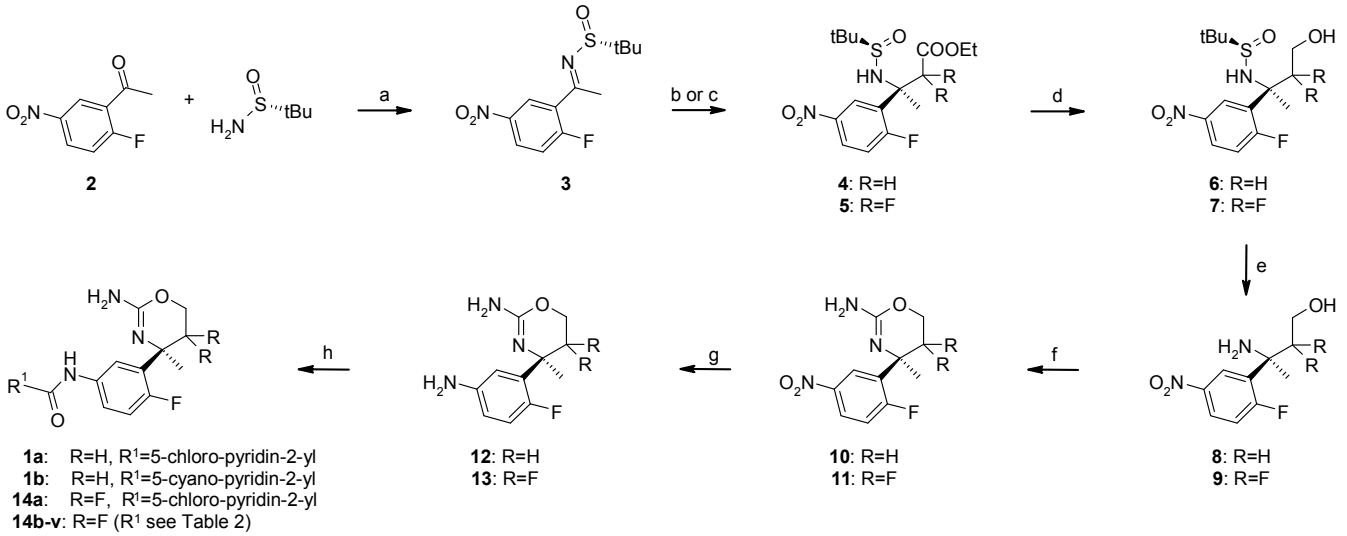

[a]Reagents and conditions: (a) $Ti(OEt)_4$, THF, 50-70 °C. (b) **3->4**: MeCOOEt, LDA, $TiCl(OiPr)_3$, THF, -78 °C. (c) **3->5**: $BrCF_2COOEt$, Zn, CuCl, THF, 35 °C. (d) $LiBH_4$, THF, 0 °C. (e) HCl/1,4-dioxane/MeOH, 22 °C. (f) BrCN, EtOH, 85 °C. (g) H_2, Pd/C, EtOH, 22 °C. (h) 4-(4,6-Dimethoxy[1.3.5]triazin-2-yl)-4-methylmorpholinium chloride hydrate (DMTMM), MeOH, 22 °C.

The ester group in **4** and **5** was then reduced to the alcohols **6** and **7** with $LiBH_4$ which was followed by cleavage of the chiral auxiliary under acidic conditions to give the amino alcohols **8** and **9**.[32] Cyclization of the amino alcohols **8** and **9** was readily accomplished with cyanogen bromide to give the oxazines **10** and **11** which were reduced to the corresponding anilines **12**[33] and **13** by catalytic hydrogenation. Amide formation was accomplished without prior protection of the amidine moiety using 4-(4,6-dimethoxy[1.3.5]triazin-2-yl)-4-methylmorpholinium chloride hydrate,[34] furnishing the target compounds **1a-b** and **14a-v** (Table 2). The absolute configurations were assigned based on X-ray structures of **1b** and **14d** complexed to BACE1.

The commercially unavailable acids **23-26** (Scheme 2), required to introduce R^1 residues in difluoro-oxazine **14** (Table 2), were made available from pyridine and pyrazine derivatives **15** and **17** via the alkylated esters **19-22**. Attempted alkylation of the hydroxy-pyrazine ester **16** with 3-bromopropyne did not lead to the expected *O*-alkylated product **22** but furnished the *N*-alkylated product (5-oxo-4-prop-2-ynyl-4,5-dihydro-pyrazine-2-carboxylic acid methyl ester, structure not shown). Compound **27** was prepared directly from the acid **18** without proceeding via the corresponding ester. Finally, chlorination of the pyrazole ester **28** with N-chlorosuccinimide followed by saponification delivered the chloro-pyrazole derivative **30**.

Scheme 2. Synthesis of Commercially Unavailable Building Blocks 23-27 and 30.[a]

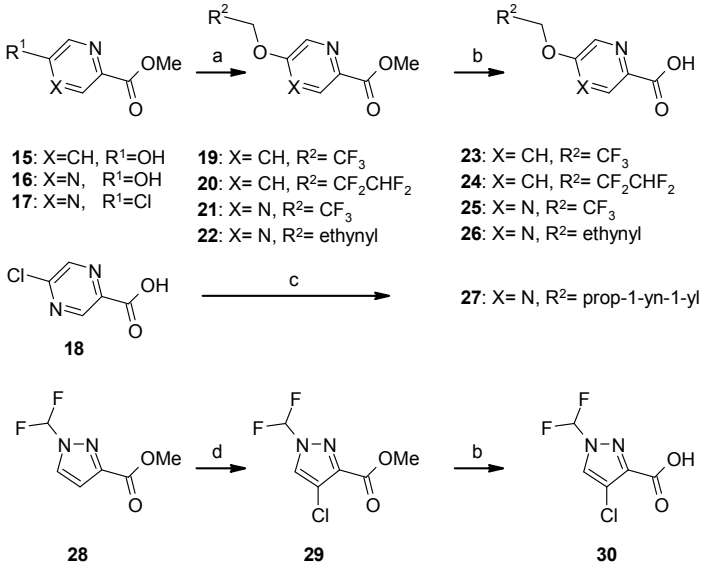

[a]Reagents and conditions: (a) **15**->**19**: CF_3CH_2OTf, NaH, DMF, 22 °C; **15**->**20**: $CHF_2CF_2CH_2OTf$, K_2CO_3, acetone; **17**->**21**: CF_3CH_2OH, Cs_2CO_3, DMF; **17**->**22**: prop-2-yn-1-ol, *tert*-BuOK, 1,4-dioxane, 22 °C. (b) LiOH or NaOH, THF/H_2O, 22 °C to reflux. (c) But-2-yn-1-ol, *tert*-BuOK, DMF, 65 °C. (d) N-chlorosuccinimide, DMF, 50 °C.

To access fluoro-oxazines **66-70** (Scheme 3) having fluorines attached at positions R^2-R^4 the synthetic strategy was modified. Occasionally the alcohol group in **6-9** (Scheme 1) can undergo an intramolecular aromatic substitution of the fluorine, which is activated by the nitro group, to give the corresponding nitro-chromane derivatives (structures not shown). We therefore introduced the nitro group at a later stage of the synthesis. The commercially unavailable ketones **34** and **35** (Scheme 3) were made available by fluorination of the alcohol **31** or by acylation of **32** using ethyl difluoroacetate. Sulfinyl imines **36-38**, prepared as described in Scheme 1, were then subjected to the Reformatsky reaction to afford the esters **39-43**. The reaction of **36** with BrCHFCOOEt yielded a separable 4:1-mixture of the epimers **39** and **40**. Conversion of **37** with BrCHFCOOEt gave a separable 8:1-mixture of **41** as the major isomer and the corresponding epimer (R^3=H, R^4=F). Oxazines **49-51** and **53-54**, prepared in analogy to Scheme 1, were then nitrated with fuming nitric acid, followed by reduction of

the nitro group and amide formation in the usual manner, to give the targeted fluorinated oxazines **66-70**. The relative and absolute configurations were assigned based on X-ray structures of **66-70** complexed to BACE1.

Scheme 3. Synthesis of Fluoro-oxazines 66-70.[a]

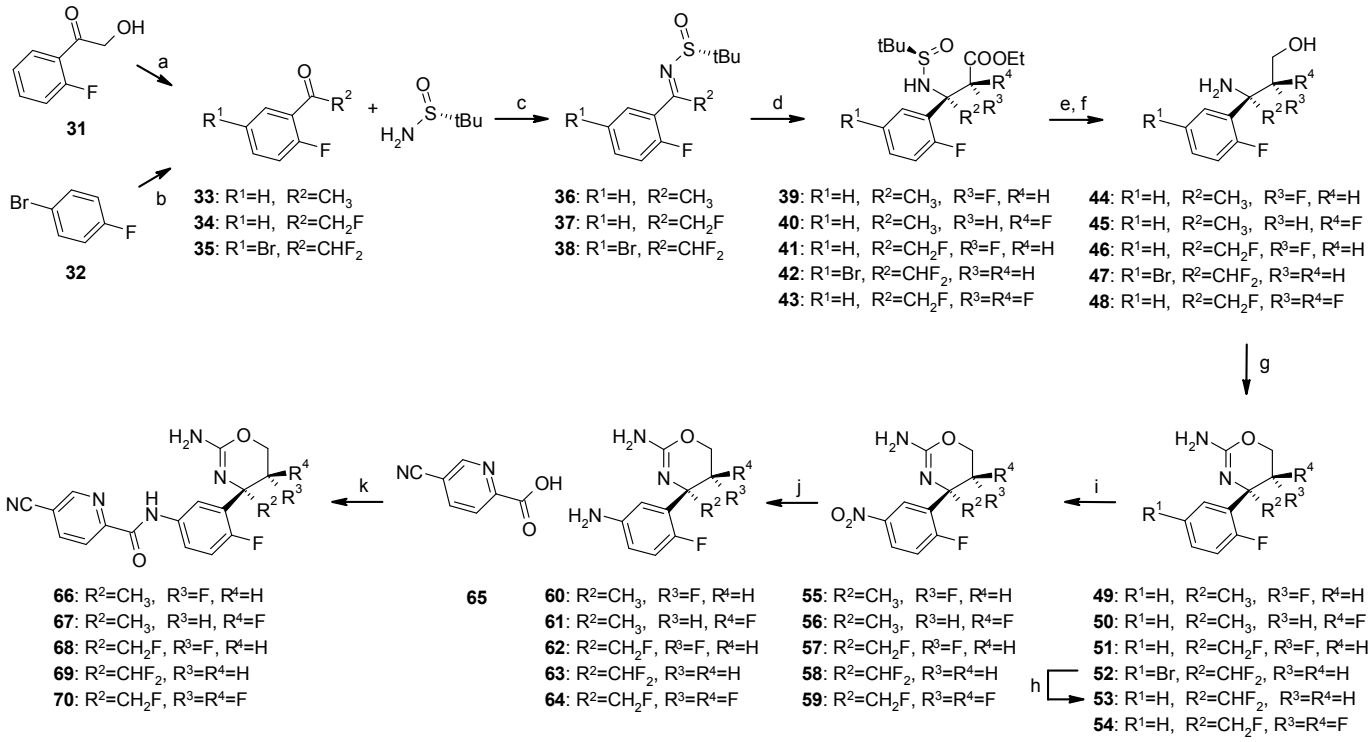

[a]Reagents and conditions: (a) **31**->**34**: Nonafluoro-n-butansulfonyl fluoride, triethylamine trihydrofluoride, CH_2Cl_2, 0 °C to 22 °C. (b) **32**->**35**: LDA, $F_2CHCOOEt$, THF, -70 to -10 °C. (c) $Ti(OEt)_4$, THF, 70 °C. (d) **39**, **40** and **41**: BrCHFCOOEt, **42**: $BrCH_2COOEt$, **43**: $BrCF_2COOEt$, Zn, CuCl, THF. (e) $LiBH_4$, EtOH, 22 °C. (f) aq. HCl, THF, 22 °C. (g) BrCN, *i*-PrOH or EtOH, 80 °C. (h) H_2, Pd/C, NaOAc, MeOH, 22 °C. (i) HNO_3, H_2SO_4, TFA, 0 °C. (j) H_2, Pd/C, Et_3N, EtOH, 22 °C. (k) DMTMM, MeOH, 0 °C to 22 °C.

The synthesis of trifluoromethyl substituted oxazines **88** and **89** (Scheme 4) required a different strategy. Ready access to CF_3 substituted 3-amino-propan-1-ol derivatives **80** and **81** is achieved using a dipolar cycloaddition reaction of a nitrile oxide and an olefin[35] as the key step. Utilizing carefully optimized conditions, the nitrile oxide was slowly generated *in situ* from 2-chloro-2-hydroxy-imino ester **71** in a heterogeneous mixture of $NaHCO_3$ in ethyl acetate in the presence of 3,3,3-trifluoropropene (**72**) to give the 4,5-dihydro-isoxazole ester **73** in quantitative yield. Reduction of the ester **73** followed by

fluorination of the alcohol **74** with Deoxo-Fluor® furnished the desired fluoro compound **75**. 3-Methyl-4,5-dihydro-isoxazole derivative **76** was directly accessible by reacting nitroethane and phenyl isocyanate to generate the nitrile oxide *in situ* in the presence of **72**. Arylation of the imines **75** and **76** with 1-bromo-2-fluoro-benzene (**77**) and *n*-BuLi occurred from the sterically less hindered side to give the racemic isoxazolidines **78** and **79**, which were separated by chiral HPLC affording the chiral compounds **78** and **79**. Transfer hydrogenation employing ammonium formate and Pd/C led to the amino alcohols **80** and **81**, which were then converted to the CF_3-substituted oxazines **88** and **89** following the procedures employed in Scheme 3. The relative and absolute configurations were assigned based on X-ray structures of **88** and **89** complexed to BACE1.

Scheme 4. Synthesis of Trifluoromethyl-oxazines 88 and 89.[a]

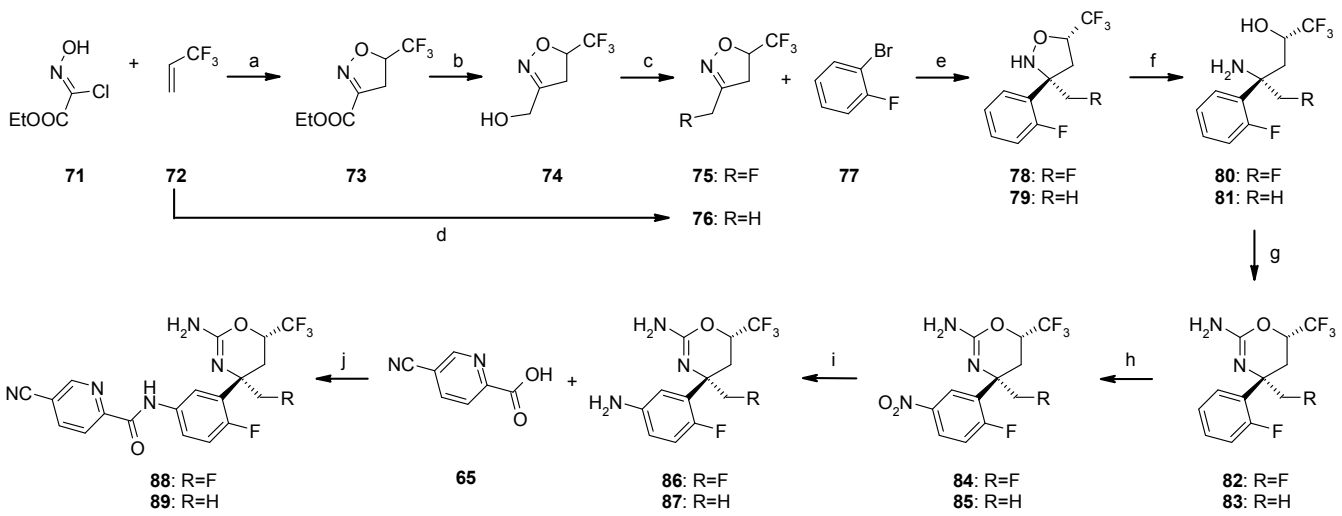

[a]Reagents and conditions: (a) $NaHCO_3$, EtOAc, -65 °C to 22 °C. (b) $NaBH_4$, EtOH, 0 °C. (c) Deoxo-Fluor®, CH_2Cl_2, -78 °C to 22 °C. (d) **72**->**76**: Nitroethane, phenylisocyanate, Et_3N (cat.), Et_2O, -78 °C to 22 °C. (e) THF, *n*-BuLi, $BF_3{\cdot}Et_2O$, -78 °C to 22 °C. (f) $HCOONH_4$, Pd/C, EtOH, 22 °C. (g) BrCN, EtOH, 85 °C. (h) H_2SO_4, HNO_3, 0 °C. (i) H_2, Pd/C, EtOH, Et_3N, 22 °C. (j) DMTMM, MeOH, 0 °C to 22 °C.

The last set of CF_3-substituted oxazines **109-111**, not accessible by methods hitherto described, again required a different synthetic strategy. Esters **90** and **39** were reduced with DIBAH at -76 °C to give the aldehydes **91** and **92** which were reacted with trimethyl(trifluoromethyl)silane (Ruppert-Prakash reagent) yielding the alcohols **93-96**. The reaction of **91** afforded a separable 1:2-mixture of epimers **93** and **94**, aldehyde **92** gave a separable 2:1-mixture of epimers **95** and **96** with inverse selectivity.

Conversion of alcohols **93**, **95** and **96** to the target compounds **109-111** followed well-established procedures as described in previous Schemes. The relative and absolute configurations were assigned based on X-ray structures of **109-111** complexed to BACE1.

Scheme 5. Synthesis of Fluoro-oxazines 109-111.[a]

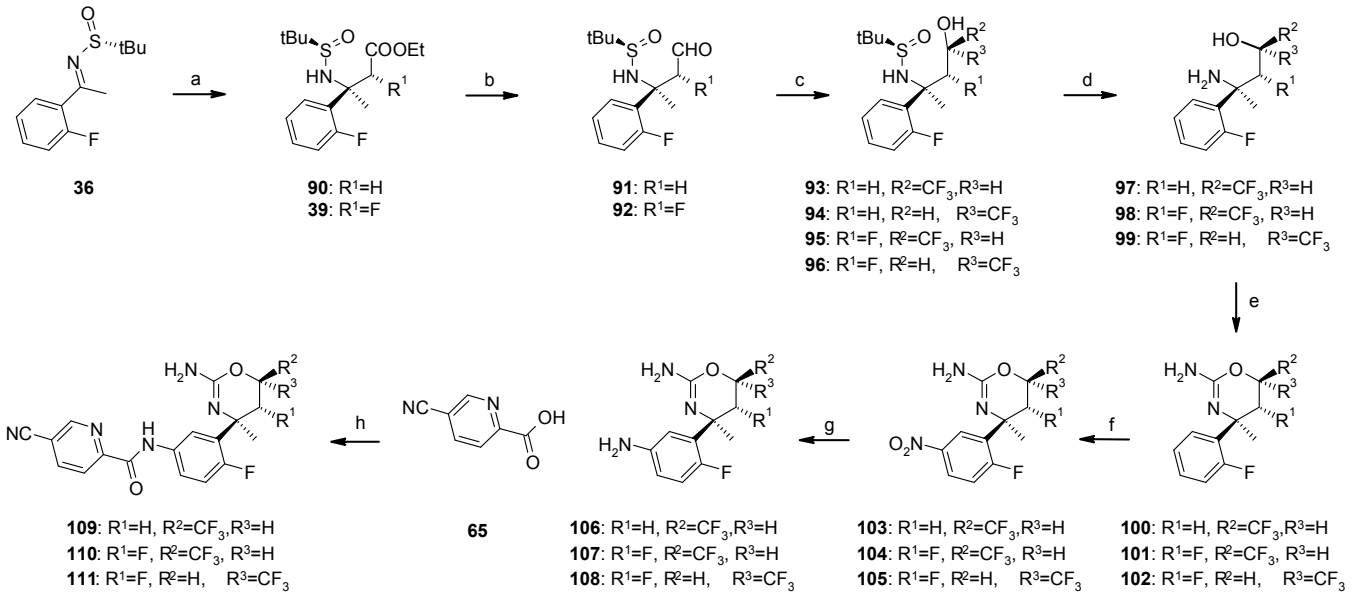

[a]Reagents and conditions: (a) **36->39**: BrCHFCOOEt, Zn, CuCl, THF; **36->90**: $BrCH_2COOEt$, Zn, CuCl, THF. (b) DIBAH, toluene, -76 °C. (c) Trimethyl(trifluoromethyl)silane, THF, TBAF, 0 °C. (d) aq. HCl, THF, 22 °C. (e) BrCN, EtOH, 85 °C. (f) H_2SO_4, HNO_3, 0 °C. (g) H_2, Pd/C, EtOH, Et_3N, 22 °C. (h) DMTMM, MeOH, 0 °C to 22 °C.

RESULTS AND DISCUSSION

At the outset of the BACE project, we envisaged both BACE1 and BACE2 as viable targets for AD and type 2 diabetes, respectively. The recently described oxazine **1a**[29, 36, 37] (for other 1,3-oxazine BACE1 inhibitors see[26, 27, 38]) looked particularly suited for the diabetes target, which is primarily expressed in peripheral tissue. Compound **1a** showed a high enzymatic inhibitory activity at BACE2 (Table 1, IC_{50}=0.052 μM) and was hardly brain penetrant as evident from the low brain/plasma ratio in mice (0.13 at 30 mg/kg) resulting in a marginal activity of 29% reduction of Aβ40 at 30 mg/kg in our wild type mice model (*vide infra*) we use for the AD indication. An undesired potential liability of **1a**, however,

was the high basicity (pKa=9.8) giving rise to potential phospholipidosis[39] and polypharmacology.[40, 41] To overcome these liabilities, we introduced fluorines into the head group[42] as depicted in difluoro-oxazine **14a**.[43] Indeed, this modification reduced the pKa by 3.5 log units compared to **1a** and improved the enzymatic potency at BACE1 and BACE2 5 and 3-fold, respectively. Unexpectedly, however, **14a** readily penetrated the brain (brain/plasma ratio in mice=2.3 at 30 mg/kg) and therefore showed good *in vivo* activity in mice with a 69% reduction of Aβ40 at 30 mg/kg. Obviously, this serendipitously found effect of fluorinated oxazines now rendered this compound class much more appropriate for the AD indication than type 2 diabetes.

Table 1. *In Vitro* and *In Vivo* Profiles of Oxazines **1a**, **14a** and Thiazines **112**, **113**.

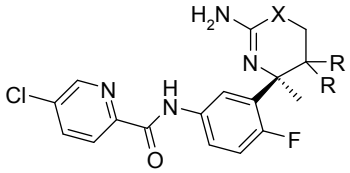

compd	X	R	pKa[b]	IC50 (μM)[a] hBACE1 enzyme	IC50 (μM)[a] hBACE2 enzyme	IC50 (μM)[a] Aβ40 cell-based[c]	shift BACE1 enzyme vs. cell-based	brain Aβ40 reduction in mice at 30 mg/kg[d]
1a	O	H	9.8	0.137	0.052	0.010	14	29%
14a	O	F	6.3	0.026	0.015	0.017	2	69%
112	S	H	9.0	0.016	0.009	0.001	16	92%
113	S	F	6.1	0.014	0.010	0.004	3	0%

[a]IC_{50} values are means of at least 2 independent experiments. [b]pKa determined by capillary electrophoresis. [c]HEK293 cells transfected with wild-type human APP. [d]Compound given orally, n=3-4, 4h post dose, mean reduction as compared to vehicle control.

For comparison, the thiazine **112**[23] and its fluorine congener **113**[32], both described by Shionogi, were also prepared. Interestingly, thiazine **112** was very potent *in vivo* (92% Aβ40 reduction at 30 mg/kg) while the oxazine **1a** was not. Most surprisingly, the fluorine congener **113**, expected to be even more potent than **112**, was inactive *in vivo*. Another remarkable difference was the impact of basicity on the shift between enzymatic and cellular BACE1 potency. Compounds **1a** and **112** with high basicity (pKa=≥9) showed a significantly higher cellular activity (14 and 16-fold, respectively) whereas compounds **14a** and **113** with low basicity (<6.5) did not (2 and 3-fold, respectively). The oxazine **14a** served as a basis for further optimization of the *in vivo* activity.

SAR of R^1 substituents. Next we explored various R^1 aromatic residues all having a nitrogen atom in *ortho* position to the amide group (Table 2) to direct the aromatic residue into the S3 pocket (*vide infra*).

Table 2. SAR of R1 Substituents and *In Vivo* Properties of Difluoro-oxazines **14a**–**v**.

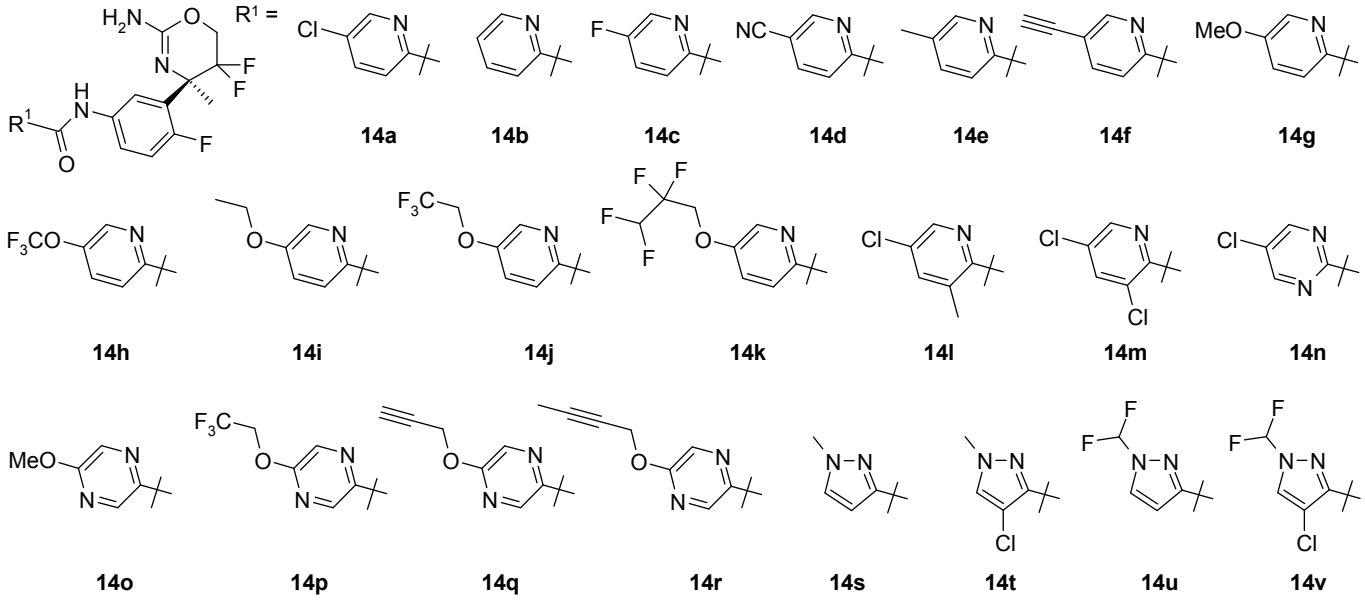

compd	IC_{50} (μM)[a] hBACE1 enzyme	IC_{50} (μM)[a] hBACE2 enzyme	selectivity BACE2/1	IC_{50} (μM)[a] Aβ40 cell-based[b]	shift BACE1 enzyme vs. cell-based	brain Aβ40 reduction in mice at 30/10 mg/kg[c]
14a	0.026	0.015	0.6	0.017	2	69% / 28%
14b	0.294	0.036	0.1	0.230	1	- / -
14c	0.066	0.022	0.3	0.013	5	- / -
14d	0.023	0.024	1	0.021	1	84% / 78%
14e	0.087	0.030	0.3	0.087	1	- / -
14f	0.032	0.047	1	0.024	1	27% / -
14g	0.051	0.045	1	0.061	1	64% / -
14h	0.057	0.245	4	0.054	1	64% / -
14i	0.184	0.904	5	0.480	-3	- / -
14j	0.108	7.490	69	0.290	-3	- / -
14k	0.042	9.440	225	0.100	-2	- / -
14l	0.017	0.010	0.6	0.016	1	- / -
14m	0.026	0.012	0.5	0.013	2	91% / 77%
14n	0.067	0.023	0.3	0.023	3	- / -
14o	0.027	0.119	4	0.022	1	95% / 66%
14p	0.025	0.943	38	0.110	-4	- / -
14q	0.013	0.175	13	0.001	13	98% / 93%
14r	0.006	0.101	17	0.001	6	94% / 28%
14s	0.446	0.106	0.2	0.110	4	- / -
14t	0.151	0.031	0.2	0.131	1	- / -
14u	0.036	0.018	0.5	0.017	2	- / -
14v	0.019	0.011	0.6	0.013	1	57% / -

[a]IC_{50} values are means of at least 2 independent experiments. [b]HEK293 cells transfected with wild-type human APP [c]Compound given orally, n=3-4, 4 h post dose, mean reduction as compared to vehicle control.

Out of a number of 6-membered heterocycles explored, pyridines, pyrimidines and pyrazines showed promising *in vitro* activities. Pyridines **14a–k** having one substituent in *para* position to the amide showed enzymatic inhibition at IC_{50s} values below 0.3 uM, most of them with good cellular activity. The nitrile **14d** displayed already an improved *in vivo* activity compared to the chloride **14a** with Aβ40 reductions of 78 and 28%, respectively at a dose of 10 mg/kg. In addition, favorable mouse PK data for **14d** (Cl=22 ml/min/kg, $T_{1/2}$=1.8 h, Vss=2.9 L/kg, F=52%) encouraged us to explore further substitution patterns. The *o*- and *p*-disubstituted pyridines **14l** and **14m** were virtually equipotent to the mono substituted chloride **14a** both in the enzymatic as well as the cell-based assay, but **14m** showed a higher *in vivo* activity compared to **14a** (77% vs. 28% reduction of Aβ40 at 10 mg/kg). The pyrimidine **14n** was 3-fold less active in terms of enzymatic potency compared to the pyridine **14a**. Pyrazines **14o–14r** showed good enzymatic inhibition activity (IC_{50}=0.027-0.006 μM), and examples **14o** and **14p** were clearly more potent in the enzyme/cell-based assays compared to their corresponding pyridine counterparts **14g** (2/3-fold) and **14j** (4/3-fold), respectively. Interestingly, the propynyloxy-pyrazine **14q** was very potent *in vivo* (93% reduction of Aβ40 at 10 mg/kg). Out of a number of 5-membered aromatic heterocycles explored, pyrazoles looked particularly promising. A first example, the methyl pyrazole **14s**, was only moderately active in the enzyme/cell-based assays (IC_{50}=0.446/0.110 μM) and showed very low metabolic stability in mouse microsomes (Cl=200 μL/min/mg protein). Potential labile positions, i.e. the methyl group and position 4 of the pyrazole, were therefore blocked by fluorines and a chlorine substituent, respectively. As expected, metabolic stability in mouse microsomes improved considerably in **14t-v** (Cl=98, 59 and 9 μL/min/mg protein, respectively) and higher enzymatic potencies were also observed (IC_{50}=0.151, 0.036 and 0.019 μM, respectively). Disappointingly, however, the *in vivo* activity of **14v** remained rather modest, with a 57% reduction of Aβ40 at 30 mg/kg. The shift between enzyme and cell-based activity was in the majority of examples rather small (6-fold and less,

with the exception of a 13-fold shift of the alkyne derivative **14q**) and in general in favor of higher cellular activity. The (fluoro)alkoxy derivatives **14i**-**14k** and **14p**, however, were found to have "negative" shifts (2 to 4-fold) in favor of higher enzymatic potencies clearly demonstrating that not only the pKa but also the nature of R^1 substituents had an impact on the shift.

X-ray structures and BACE2 selectivity. The catalytic aspartate residues D93 and D289 form the central recognition motif in the BACE1 binding site (Figure 2). The active site is partially covered by a flexible hairpin loop commonly referred to as the "flap" (Y129 - E138).[44] In apo structures of BACE1 or in complexes with small molecule inhibitors containing an amidine binding motif, the flap backbone is approximately 12 Å away from the side-chains of D93 and D289 (the "open" position). In complexes with peptidomimetic transition state analogs the flap moves approx. 4 Å closer to the binding site (the "closed" position).[44] There is an additional flexible region, the "10s loop"[44] (G69 – G74) forming one side of the S3 pocket. In BACE1 the 10s loop is either in an "up" or "down" conformation,[45] whereas in BACE2 the 10s loop has been observed in a down conformation by Ostermann et al.[46] and by ourselves in the complex with **14i** (Figure 3). The S3 pocket is much larger in the up conformation, so this difference can be exploited to modulate BACE1/2 selectivity as well as selectivity against other single chain aspartyl proteases.[44] The binding pocket in S1 and the region at the catalytic aspartates are almost identical between BACE1 and BACE2. Conformational variation around the active site of BACE1 has recently been discussed in detail by Xu et al:[47] we will analyze BACE2 flexibility in detail separately.[48]

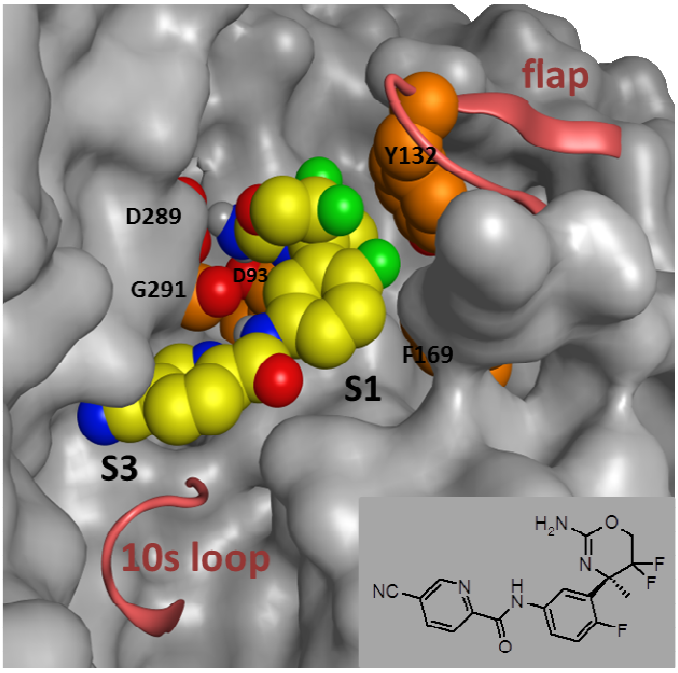

Figure 2. 14d bound to the BACE1 binding site. The amidine recognition motif is tightly bound to the catalytic aspartates D289 and D93 (partially hidden) in the bottom of the pocket. The fluorine atoms in the head group and the *o*-F substituent of the phenyl ring (marked in green) form a network of vdW interactions to Y132 and to F169. An additional H-bond is established between the NH of the amide bond of the ligand and the backbone carbonyl oxygen of G291. The *para* nitrile substituent displaces bound water molecules from the S3 pocket.

In Figure 2 the topology of the BACE1 active site bound to **14d** is highlighted. Tight hydrogen bonds are formed between the protonated amidine motif in the oxazine head group and the catalytic aspartates. The fluorine atoms in position 5 and the *o*-F substituent of the phenyl ring (S1 pocket) are engaged in a network of van-der-Waals interactions to Y132 located in the flap and to F169 at the rim of the S1 pocket. A hydrogen bond is formed between the NH of the amide bond in **14d** and the backbone carbonyl oxygen of G291. The *para* nitrile substituent projects into the S3 pocket and displaces bound water molecules seen in the apo structure, thereby enhancing binding affinity. The proper orientation in the S3 pocket is supported by a stabilization of the conformation of the pyridine ring via a favorable electrostatic interaction between the pyridyl N and the NH of the amide bond in **14d**.

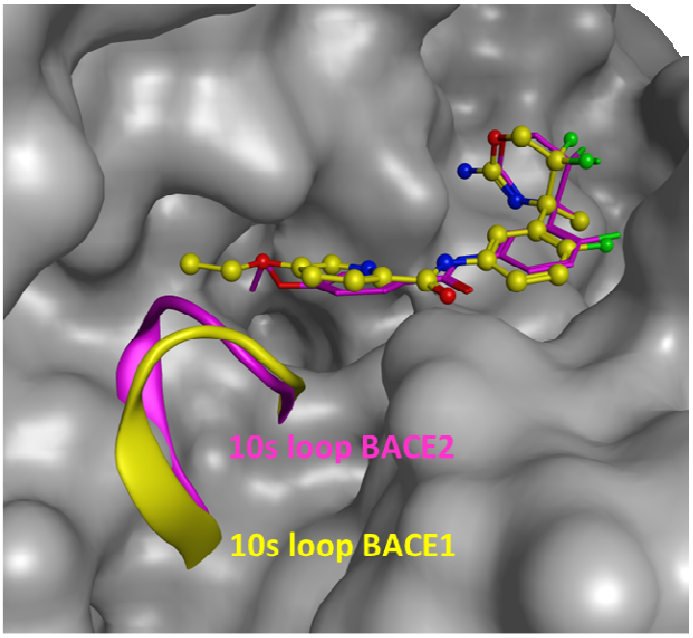

Figure 3. 14i bound to BACE1 (yellow, ball and stick representation) and BACE2 (magenta, stick representation). The molecular surface has been generated for BACE1, the 10s loops of BACE1 and BACE2 are depicted separately. The ethoxy sidechain in **14i** prefers a planar orientation around the C-O bond. When bound to BACE2 the corresponding torsion angle deviates significantly from planarity, since the S3 pocket in BACE2 is tighter than in BACE1 due to the "down" conformation of the 10s loop in BACE2.

The role of the 10s loop in modulating BACE1/2 selectivity can be seen in the ratios of inhibition constants of the compounds **14g-k** (Table 2). As it is evident in Figure 3, the S3 pocket in BACE2 is smaller than in BACE1, because the 10s loop in BACE2 is observed here in a down conformation. The IC_{50} ratio between BACE2 and BACE1 increases with the growing chain length of the S3 alkyl substituent. Longer chain lengths can only be accommodated in the BACE2 S3 pocket by adopting an unfavorable ligand conformation as depicted in Figure 3. The ethoxy sidechain in **14i** prefers a planar orientation around the C-O bond. When bound to BACE2 the corresponding torsion angle deviates significantly from planarity, and this conformational strain translates into a reduced inhibition of BACE2. A similar rationale applies for the increase in selectivity with an increasing number of F substituents. In order to avoid repulsive contacts between F-substituents and carbonyl oxygen atoms of the protein, the tighter S3 pocket in BACE2 requires more strained conformations of the S3 substituent than the more spacious pocket in BACE1.

Fluorine scan of oxazines. From various R1 aromatic residues explored, we selected the nitrile **14d** for further optimization based on its balanced profile, i.e. good *in vitro* activities, no shift between enzymatic and cell-based assay and a favorable *in vivo* activity. The crucial role of the pKa on the pharmacological profile as found in the difluoro-oxazine **14a** prompted us to investigate extensively the impact of fluorines on various parameters. Oxazines with fluorines appended at different positions in the head group (Table 3) were prepared spanning a pKa range of almost five log units. The head groups in Table 3 are ordered according to decreasing pKa values. Below we discuss the impact of fluorines on the pKa, the lipophilicity, the enzymatic potency, the shift of enzyme vs. cell-based activity, P-gp efflux and hERG inhibition, most of these parameters eventually affecting *in vivo* activity.

Table 3. Head Group Fluorine Scan and *In Vitro*/*In Vivo* Properties of Fluorinated Oxazines.

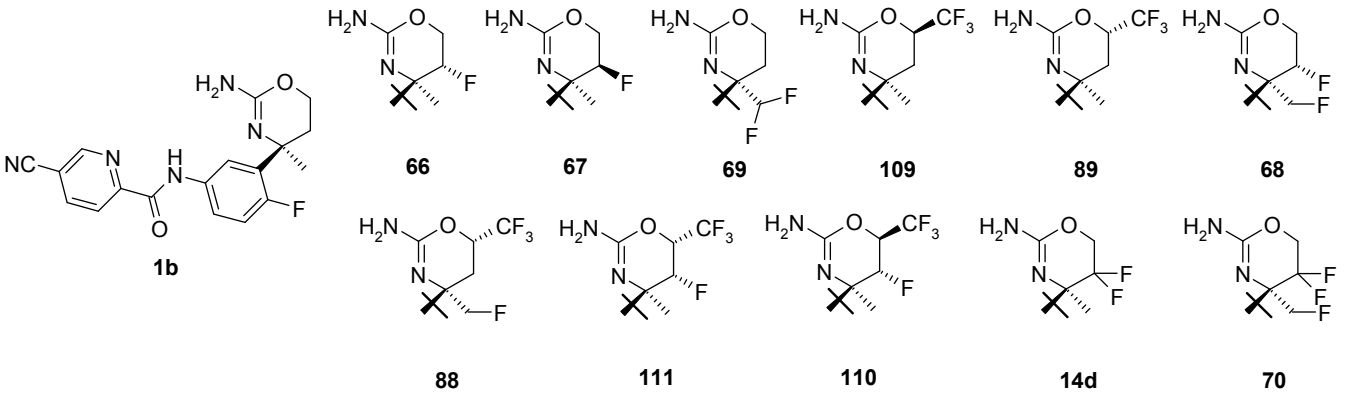

compd	pKa[b]	Δ pKa to **1b**	logD[c]	logP	Δ logD/logP	IC50 (μM)[a] hBACE1 enzyme	IC50 (μM)[a] Aβ40 cell-based[d]	shift BACE1 enzyme vs. cell-based	P-gp ER[e]	hERG inhibition at 10μM	brain Aβ40 reduction in mice at 10/3/1 mg/kg[f]
1b	9.7	0	0.0	2.3	2.3	0.051	0.014	4	14.8	88%	13% / - / -
66	8.1	-1.6	1.1	1.9	0.8	0.028	0.001	28	4.9	85%	89% / 43% / -
67	7.4	-2.3	1.3	1.6	0.3	0.435	0.027	16	2.1	91%	2% / - / -
69	7.3	-2.4	1.7	1.9	0.2	0.054	0.009	6	1.7	85%	68% / 34% / -
109	7.3	-2.4	2.8	3.1	0.3	0.776	0.230	3	-	-	- / - / -
89	7.0	-2.7	2.8	2.9	0.1	0.012	0.002	6	1.9	75%	95% / 88% / 78%
68	6.7	-3.0	1.6	1.7	0.1	0.077	0.025	3	2.6	65%	55% / 26% / -
88	6.3	-3.4	3.0	3.0	0	0.019	0.013	1	1.6	39%	88% / 64% / 11%
111	5.9	-3.8	3.1	3.1	0	0.013	0.010	1	1.5	48%	93% / 71% / 41%
110	5.8	-3.9	3.1	3.1	0	0.040	0.150	-4	1.5	-	- / - / -
14d	5.8	-3.9	2.5	2.5	0	0.023	0.021	1	1.5	43%	78% / 39% / 4%
70	5.1	-4.6	2.3	2.3	0	0.049	0.400	-8	1.6	14%	- / - / -

[a]IC_{50} values are means of at least 2 independent experiments. [b]pKa determined by capillary electrophoresis. [c]LogD determined in 1-octanol/phosphate buffer, pH=7.4. [d]HEK293 cells transfected with wild-type human APP. [e]ER=efflux ratio

in LLC-PK1cells stably expressing human MDR1. [f]Compound given orally, n=3-4, 4 h post dose, mean reduction as compared to vehicle control.

The configuration of a fluorine atom attached directly to the oxazine ring has a strong impact on the pKa. Thus, the "down" configured fluorine in **66** showed a pKa decrement of 1.6 (ΔpKa of **1b** and **66**) whereas the "up" configured fluorine in **67** induced a larger pKa decrement of 2.3. Similar effects were also observed in fluoro-piperidines.[49, 50] The difluoro oxazine **14d** showed exactly the sum of both contributions, i.e. a pKa decrement of 3.9. The two fluorines in compound **69**,[37, 51] also located at the β-position to the ring nitrogen, induced a lower pKa decrement of 2.4 compared to those of difluoro oxazine **14d**. It appears that fluorines with limited conformational flexibility as present in **14d** induced a larger pKa decrement compared to those in **69** having more flexibility. The CF_3 group in compounds **109** and **89** still showed a remarkably large pKa decrement of 2.4 and 2.7, respectively, despite the longer distances through which the fluorines exert their impact on the nitrogens. This observation can be rationalized based on the equidistance of the fluorines to both nitrogens in the *δ*-position having an impact not just on one but on both nitrogens of the amidine moiety. Fluorines located at more than one position (as in **68**, **88**, **111**, **110** and **70**[51]) showed a more complex picture with pKa decrements not being additive.

The lipophilicity of compounds having 1-3 fluorines attached to the head group is reduced or similar (logP=1.6–2.5 in **66-70** and **14d**) compared to the non-fluorinated oxazine head group **1b** (logP =2.3). Compounds substituted by a CF_3 group showed increased lipophilicity (logP=2.9 – 3.1 in **88**, **89**, **109**–**111**) compared to **1b**. As expected, the Δ logP/D approaches a value of 0 at a pKa of 6.3.

The enzymatic potency was strongly affected by fluorines introduced into the oxazine head group. A down configured CF_3 group in **89** improved the binding affinity considerably (IC_{50}=0.012 μM) compared to unsubstituted **1b** (IC_{50}=0.051 μM). According to the X-ray structure, the CF_3 group does not interact with BACE1 but points towards the solvent. A possible rationale for this unexpected increase in binding affinity might be the pKa of **89**, which is 2.7 log units lower than for **1b**. Therefore,

1b should be more strongly solvated than **89** due to its higher basicity. The lower binding affinity of **1b** compared to **89** could be rationalized by the higher desolvation enthalpy upon binding to the active site. The configurations of the fluorine in **66** and the CF_3 group in **89** strongly affected the binding affinity, which increased 16-fold and 65-fold, compared to their epimers **67** and **109**, respectively. This effect can be rationalized by conformational strain of the head groups. The head groups of the X-ray structures were submitted to a semiempirical geometry optimization[52] (PM3 hamiltonian) outside the binding pocket (unbound geometry). As shown in Figure 4, the coordinates of bound as well as unbound **66** and **89** remain almost unchanged, therefore, the oxazine rings are without conformational strain. The geometry optimization of **109** resulted in a different ring pucker, indicating that the bound ligand is not in its lowest energy conformation. This conformational strain results in a reduced binding affinity. The geometry optimization of **110** also yields a strained conformation in the bound state. However, the effect on binding affinity is much lower than expected. A reason for this result might be the involvement of the F-substituent in the network of van-der-Waals interactions involving Y132, which could overcompensate the conformational energy penalty. For **67** the position of the methylene carbon next to the oxazine oxygen atom cannot be clearly assigned because of weak electron density. This is probably due to the presence of multiple ring conformations indicating that **67** is not well bound in the active site.

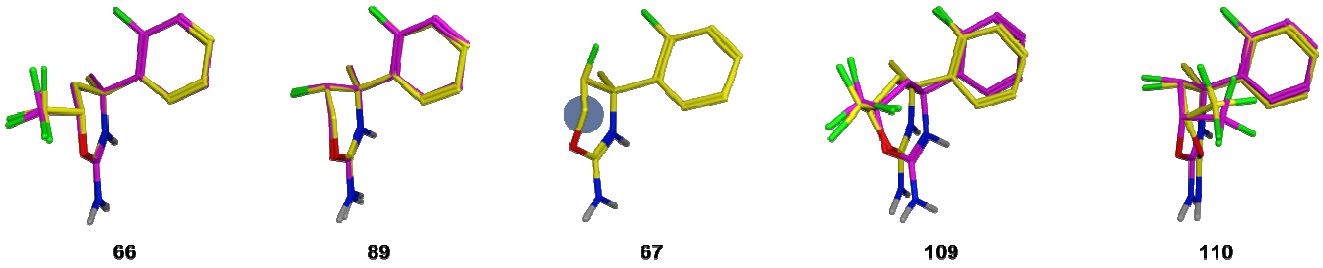

Figure 4. X-ray structures (yellow) of fluorinated head groups with the S1 phenyl ring were energy minimized in the unbound state by a semiempirical geometry optimization with the PM3 hamiltonian (magenta). The coordinates of **66** and **89** remain almost unchanged as compared to the bound conformation. Therefore, the oxazine rings are without conformational strain. The geometry optimization of unbound **109** and **110** resulted in different ring puckers indicating that those ligands are not in their lowest energy conformations. For **67** the position of the marked C-atom cannot be clearly assigned because of weak electron density. This indicates the presence of multiple ring conformations.

The shift of cellular vs. enzymatic activity depends on the pKa: basic compounds with a pKa ≥7 show a trend for higher activity in the cell-based assay whereas oxazines with a pKa <7 are more balanced or can even revert to have a higher potency in the enzymatic assay.[53] BACE1 inhibitors with enhanced basicity have been associated with increased cellular potency by favoring the acidic intracellular compartment where BACE1 is located.[54]

P-gp mediated efflux is clearly correlated with the pKa.[55] Lowering of the pKa from 9.7 to 8.1 to 7.4 in compounds **1b**, **66** and **67** resulted in a continuous reduction of the efflux ratio from 15 to 5 to 2, respectively, which remained low at a pKa <7.4. There was in general no species differences between human and mouse P-gp efflux, e.g. for compound **89** (efflux ratio=1.9/1.9, respectively) and compound **14d** (efflux ratio=1.5/2.3, respectively).

hERG inhibition is strongly affected by the pKa.[56] Reduction of the pKa from 9.7 to 5.1 correlated well with hERG inhibition which declined from 88 to 14% at 10 μM.

The low *in vivo* activity of compound **1b** (13% reduction of Aβ40 at 10 mg/kg) is now better understood because of the high P-gp efflux ratio of 15. Attachment of one fluorine in the relaxed down configuration in compound **66** boosted the cellular activity 14-fold and reduced P-gp efflux 3-fold as compared to **1b** resulting in good *in vivo* activity (43% reduction of Aβ40 at a lower dose of 3 mg/kg). The cellular activity of compounds **88** and **111** (IC_{50}=0.013 and 0.010 μM) was lower compared to **66** (IC_{50}=0.001 μM) but the 3-fold lower P-gp efflux of 1.6/1.5 may account for the higher *in vivo* activity (64 and 71% reduction of Aβ40 at 3 mg/kg) compared to **66**. Most gratifyingly, the CF_3 substituted oxazine **89** with combined favorable properties (cellular IC_{50}=0.002 μM, P-gp efflux of 1.9) was most potent showing a reduction of Aβ40 of 78% at a dose as low as 1 mg/kg.

***In vivo* Pharmacokinetics (PK) and Pharmacodynamics (PD) of Oxazine 89.** The oxazine **89** was selected for further investigation of pharmacokinetic and dynamic parameters. Aβ40 lowering was determined after oral administration in wild-type mice (C57Bl/6J mice, n=3-4) 4 h post dosing. Wild-type mice were used as they have a normal physiological level of APP expression and are thus expected

to provide a better physiological model for Aβ-peptide production than APP-transgenic organisms. Compound **89** showed a dose-dependent inhibition of Aβ40 production in the brain of mice (Figure 5a) with a brain/plasma ratio of 1-1.5 between 0.3 and 3 mg/kg gradually increasing to 2.3 and 3.4 at the higher doses of 10 and 30 mg/kg. In a rat PK experiment (Table 4), oxazine **89** showed a low to moderate systemic plasma clearance (16.8 ml/min/kg), a high volume of distribution (11.5 L/kg) and a long terminal half-life time (9-11 h). This, together with a good oral bioavailability (68%) and a moderately high fraction unbound (20.5% in plasma) would predict a favorable PD effect in rats.

Table 4. Pharmacokinetic Properties of Oxazine 89 in Rats.[a]

dose (mg/kg)	AUC_{inf} (ng*h/mL)	Cl (ml/min/kg)	Vd_{SS} (L/kg)	$t_{1/2}$ (h)	*F* (%)	Fu[c] (%)
1.2 mg iv[b]	1195	16.8	11.5	8.9	-	-
5.2 mg po[b]	3520	-	-	10.9	68	20.5

[a]All values given are means of 2 experiments. [b]Po: Microsuspension of **89** in gelatine/aqueous NaCl; Iv: Solution of **89** in aqueous NaCl/N-methyl-2-pyridone. [c]Fu=fraction unbound.

Wild-type Wistar rats were used with a cannula inserted into the Cisterna magna and the kinetics of changes in the CSF Aβ40/42 in an acute treatment study was followed.[57] An oral dose as low as 1 mg/kg (Figure 5b) was sufficient to induce a long lasting effect, with CSF levels remaining most inhibited 4 h post dosing and still showing a significant reduction of Aβ40/42 after 24 h as a result of favorable PK properties.

The changes in plasma Aβ40/42 (Figure 5b) were analyzed in relation to the measured plasma exposure in rats (Table 4). For the modeling of the plasma exposure data, a 1-compartment model with first-order drug absorption and elimination was considered. For the modeling of Aβ40/42 changes in plasma, an indirect response model was considered with the zero-order production rate being modulated by the pharmacological effects of the oxazine **89**. The proposed model fitted the data well and the *in vivo* potency was estimated to be 0.020 μM free, which compares favorably to the *in vitro* measurement of IC_{50}=0.012 μM in the hBACE1 enzyme assay. Thus, it can be concluded that the free plasma concentration of **89** equals the free brain concentration, which can be considered as the pharmacological relevant concentration.

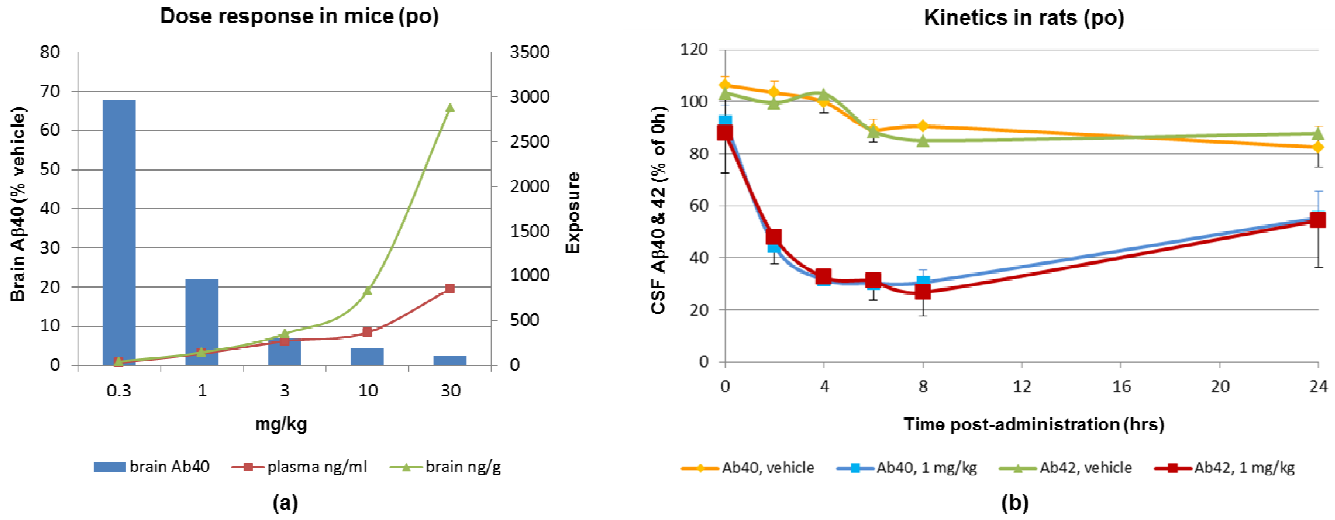

Figure 5. (a) Dose dependent inhibition of brain Aβ40 production in mice by compound **89** determined 4 h oral post dose, n=3-4, mean reduction as compared to vehicle control. **(b)** Time dependent inhibition of CSF Aβ40/42 production in rats after an oral dose of 1 mg/kg of compound **89**, n= 2-3. CSF was sampled at -1 and 0 h to define an average Aβ40/42 level for each individual rat; all post-treatment Aβ-levels were expressed as percentage of this pretreatment average.

In terms of its *in vitro* toxicological profile, compound **89** did not inhibit CYP_{450} 3A4, 2D6 and 2C9 (IC_{50} > 25μM) nor was there a time-dependent inhibition of CYP_{450} 3A4. Furthermore, **89** was very selective against other aspartyl proteases such as human Cathepsin D/E and the peptidases renin and pepsin (IC_{50} > 200μM).

SUMMARY AND CONCLUSION

Starting from a very basic, *in vivo* marginally active, 1,3-oxazine **1a**, the introduction of two fluorine atoms into the head group reduced the pKa considerably and led unexpectedly to good *in vivo* activity, as found in compound **14a**. Encouraged by this finding, we performed an extensive fluorine scan to study the impact of fluorine(s) on the pKa and a number of other parameters. Lowering the pKa had a profound effect on enzymatic and cellular activity, hERG activity, P-gp efflux and eventually on *in vivo* activity. The knowledge acquired by the fluorine head group scan delivered crucial information on how to improve *in vivo* efficacy and reduce *in vitro* toxicological liabilities. The CF_3-substituted oxazine **89** was found to be an orally active BACE1 inhibitor with an excellent PD profile in mice and a long lasting

Aβ40/42 reduction in the CSF of rats at a dose as low as 1 mg/kg. A compound from this chemical class is currently undergoing clinical evaluation for the treatment of Alzheimer's Disease.

EXPERIMENTAL SECTION

General. All solvents and reagents were obtained from commercial sources and were used as received. All reactions were followed by TLC (TLC plates F254, Merck) or LCMS (liquid chromatography-mass spectrometry) analysis. Silica gel chromatography was either performed using cartridges packed with silica gel (ISOLUTE® Columns, TELOS™ Flash Columns) or silica-NH_2 gel (TELOS™ Flash NH_2 Columns) on ISCO Combi Flash Companion or on glass columns on silica gel 60 (32-60 mesh, 60 Å). Proton NMR spectra were obtained on Bruker Avance 300, 400 or 600 MHz spectrometer with chemical shifts (δ in ppm) reported relative to tetramethylsilane or the residual solvent peak as the internal reference (i.e. $CDCl_3$ = 7.26 ppm, DMSO-d_6 = 2.50 ppm) as the internal reference. ^{1}H resonances are reported to the nearest 0.01 ppm. NMR abbreviations are as follows: s, singlet; d, doublet; t, triplet; q, quadruplet; quint, quintuplet; sext, sextuplet; m, multiplet; br, broadened. Coupling constants (*J*) are reported to the nearest 0.1 Hz. Purity was analyzed by reverse phase HPLC and for specific compounds by elemental analysis. HPLC was performed on Finnigan LTQ (Thermo Fisher Scientific) and Agilent RRLC 1200 equipment. Column: Agilent XDB C15, 30 mm x 4.6 mm, 3.5 µm. Analytical conditions: gradient used: 5% to 95% acetonitrile in water containing 0.1% trifluoroacetic acid in 3 min. Flow: 4.5 mL/min. UV-Detector: DAD 190-400 nm. Sample solvent: in water/acetonitrile (8/2). The UV detection was an averaged signal from wavelengths of 190-400 nm. Elemental analyses were performed by Solvias AG (Mattenstrasse, Postfach, CH-4002 Basel, Switzerland). Mass spectra were recorded on an SSQ 7000 (Finnigan-MAT) spectrometer for electron impact ionization. The purities of final test compounds as measured by HPLC were found to be above 95%. Melting points were determined on a Büchi Melting Point B-540: heating rate 1 °C/min starting 15 °C below melting point. LC-HRMS spectra were recorded with an Agilent LC-system consisting of an Agilent 1290 high pressure system, a CTC PAL auto sampler and an Agilent 6520 QTOF. The separation was achieved on a Zorbax Eclipse

Plus C18 1,7 µm 2.1*30mm column at 55 °C; eluent A=0.01% formic acid in Water; B= 0.01% formic acid in acetonitrile : 2-propanol (8:2); flow: 1 mL/min. Gradient: 0 min 5% of B, 0.3 min 5% of B, 4.5 min 99 % of B, 5 min 99% of B. The injection volume was 2 µL. All assay compounds had a purity of >95%. LC-MS (ESI, positive or negative ion) data were recorded on Waters UPLC-MS Systems equipped with Waters Acquity, a CTC PAL auto sampler and a Waters SQD single quadrupole mass spectrometer using ES ionization modes (positive and/or negative). The separation was achieved on a Zorbax Eclipse Plus C18 1,7 µm 2.1*30mm column at 50 °C; A=0.01% formic acid in water, B= acetonitrile at flow 1; gradient: 0 min 3%B, 0.2 min 3%B, 2 min 97 %B, 1.7 min 97%B, 2.0 min 97%B. The injection volume was 2 µL. MS (ESI, positive or negative ion): FIA (flow injection analysis)-MS were recorded on a AppliedBiosystem API150 mass spectrometer. Sample introduction was made with a CTC PAL auto sampler and a Shimadzu LC-10ADVP Pump. The samples were directly flushed to the ESI source of the mass spectrometer with a flow 50 µL/min of a mixture of acetonitrile and 10 mM ammonium acetate (1:1) without a column. The injection volume was 2 µL.

(*R*)-2-Methyl-propane-2-sulfinic acid [1-(2-fluoro-5-nitro-phenyl)-(*E*)-ethylidene]-amide (3).[32] To a solution of the (R)-(+)-tert-butylsulfinamide (10.88 g, 89.8 mmol) in THF (400 mL) was added subsequently 1-(2-fluoro-5-nitro-phenyl)-ethanone (**2**) (16.45 g, 89.8 mmol) and titanium(IV)ethoxide (40.70 g, 178.4 mmol) and the solution was stirred at reflux temperature for 5 h. The mixture was cooled to 22 °C, treated with brine (400 mL), the suspension was stirred for 10 min and filtered over Dicalite®. The layers were separated, the aqueous layer was extracted with EtOAc, the combined organic layers were washed with water, dried and evaporated. The residue was purified by flash column chromatography on silica gel using a mixture of cyclohexane/EtOAc (2:1) to give the title compound **3** (21.56 g, 84%) as a pale yellow solid: m.p. 83-85°C. ^{1}H NMR (600 MHz, $CDCl_3$) δ ppm 8.57 (dd, *J*=6.3, 2.9 Hz, 1 H), 8.33 (ddd, *J*=9.0, 3.2, 3.1 Hz, 1 H), 7.30 (t, *J*=9.5 Hz, 1 H), 2.82 (d, *J*=3.5 Hz, 3 H), 1.34 (s, 9 H). MS (ISP): *m/z* = 287.0 $[M+H]^+$. Anal. ($C_{12}H_{15}FN_2O_3S$) calcd C 50.34%, H 5.28%, N 9.78%, S 11.20%; found C 50.49%, H 5.02%, N 9.94%, S 11.31%.

(*R*)-2,2-Difluoro-3-(2-fluoro-5-nitro-phenyl)-3-((*R*)-2-methyl-propane-2-sulfinylamino)-butyric acid ethyl ester (5).[32] In a dry apparatus a suspension of freshly activated zinc powder (37.5 g, 574 mmol) and CuCl (5.99 g, 60.5 mmol) in dry THF (100 mL) was heated under an inert atmosphere to reflux for 30 min. The suspension was cooled to 22 °C treated with a solution of ethyl 2-bromo-2,2-difluoroacetate (30.7 g, 151 mmol) in dry THF (50 mL) over 1 h, and stirring was continued for 30 min. The black mixture was treated with a solution of (R)-2-methyl-propane-2-sulfinic acid [1-(2-fluoro-5-nitro-phenyl)-(E)-ethylidene]-amide (**3**) (17.5 g, 60.5 mmol) in THF (50 mL), and stirring was continued at 22 °C for 2h. The suspension was filtered through Dicalite® and washed with t-butyl methyl ether. The combined filtrates were subsequently washed with aqueous citric acid (5%) and aqueous saturated $NaHCO_3$ solution, the organic layer was dried over Na_2SO_4, filtered and the filtrate was evaporated. The residue was purified by flash column chromatography on silica gel using a mixture of n-heptane/EtOAc (2:1) to give the title compound **5** (17.24 g, 69%) as a yellow oil. ^{1}H NMR (300 MHz, $CDCl_3$) δ ppm 8.51 (dd, *J*=6.6, 2.7 Hz, 1 H), 8.29 (ddd, *J*=9.1, 3.8, 3.0 Hz, 1 H), 7.26 (dd, *J*=11.3, 9.1 Hz, 1 H), 4.72 (s, 1 H), 4.34 (qd, *J*=7.2, 1.5 Hz, 2 H), 2.09-2.17 (m, 3 H), 1.32 (t, *J*=7.3 Hz, 3 H), 1.32 (s, 9 H). MS (ISP): *m/z* = 411.2 $[M+H]^+$. Anal. ($C_{16}H_{21}F_3N_2O_5S$) calcd C 46.82%, H 5.16%, N 6.83%, S 7.81%; found C 46.73%, H 4.89%, N 6.81%, S 7.66%. The configuration of the newly introduced stereogenic center was confirmed by X-ray crystallographic analysis of the target compound **14d** complexed with BACE1 (3ZMG).

(*R*)-2-Methyl-propane-2-sulfinic acid [(*R*)-2,2-difluoro-1-(2-fluoro-5-nitro-phenyl)-3-hydroxy-1-methyl-propyl]-amide (7).[32] To a solution of (R)-2,2-difluoro-3-(2-fluoro-5-nitro-phenyl)-3-((R)-2-methyl-propane-2-sulfinylamino)-butyric acid ethyl ester (**5**) (3.78 g, 9.2 mmol) in dry THF (24 mL) was added at 0 °C lithium borohydride (9.0 mmol), and stirring was continued at 0 °C for 1.5 h. The reaction mixture was quenched by addition of acetic acid (1 mL) and water, the mixture was extracted with EtOAc, the organic layers were washed with brine, dried over Na_2SO_4 and evaporated. The residue was purified by flash column chromatography on silica gel using a mixture of n-heptane/EtOAc (3:2) to give the title compound **7** (2.90 g, 86%) as a pale yellow solid: ^{1}H NMR (600 MHz, $CDCl_3$) δ ppm 8.46

(dd, *J*=6.8, 2.8 Hz, 1 H), 8.25 (ddd, *J*=9.0, 3.7, 2.9 Hz, 1 H), 7.25 (dd, *J*=11.7, 9.0 Hz, 1 H), 5.36 (br s, 1 H), 4.51–5.03 (br s, 1 H), 4.21 (ddd, *J*=25.0, 13.4, 2.7 Hz, 1 H), 3.84 (td, *J*=12.8, 7.9 Hz, 1 H), 2.19 (s, 3 H), 1.31 (s, 9 H). MS (ISP): *m/z* = 369.0 $[M+H]^+$. A small sample was recrystallized from EtOAc/n-heptane: m.p. 154-155 °C. Anal. ($C_{14}H_{19}F_3N_2O_4S$) calcd C 45.65%, H 5.20%, N 7.60%, S 8.70%; found C 45.60%, H 5.07%, N 7.79%, S 8.78%.

(*R*)-3-Amino-2,2-difluoro-3-(2-fluoro-5-nitro-phenyl)-butan-1-ol (9).[32] A solution of (R)-2-methyl-propane-2-sulfinic acid [(R)-2,2-difluoro-1-(2-fluoro-5-nitro-phenyl)-3-hydroxy-1-methyl-propyl]-amide (**7**) (3.79 g, 10.3 mmol) in MeOH (50 mL) was treated with a solution of HCl in 1,4-dioxane (4 M, 13 mL), and stirring was continued at 22 °C for 1 h. The mixture was evaporated, the residue partitioned between EtOAc and aqueous Na_2CO_3-solution (2 M), the organic layers were washed with brine, dried over Na_2SO_4, filtered and evaporated to give the crude title compound **9** (2.50 g, 92%) as a pale yellow solid which was used without further purification . ^{1}H NMR (600 MHz, $CDCl_3$) δ ppm 8.49 (dd, *J*=7.0, 2.8 Hz, 1 H), 8.25 (ddd, *J*=9.0, 3.8, 2.9 Hz, 1 H), 7.25 (dd, *J*=11.5, 9.0 Hz, 1 H), 4.02 (ddd, *J*=19.7, 12.7, 8.6 Hz, 1 H), 3.86 (dd, *J*=23.5, 11.8 Hz, 1 H), 2.01–3.63 (3 H), 1.85 (d, *J*=0.9 Hz, 3 H). MS (ISP): *m/z* = 265.1 $[M+H]^+$. A small sample was triturated with 2-propanol: m.p. 110-111 °C. Anal. ($C_{10}H_{11}F_3N_2O_3$) calcd C 45.46%, H 4.20%, N 10.60%; found C 45.67%, H 4.20%, N 11.03%.

(*R*)-5,5-Difluoro-4-(2-fluoro-5-nitro-phenyl)-4-methyl-5,6-dihydro-4H-[1,3]oxazin-2-ylamine (11).[33] To a solution of (R)-3-amino-2,2-difluoro-3-(2-fluoro-5-nitro-phenyl)-butan-1-ol (**9**) (1.5 g, 5.7 mmol) in EtOH (30 mL) at 22 °C was added under argon cyanogen bromide (0.91 g, 8.6 mmol), and the light yellow solution was stirred in a sealed tube at 85 °C for 24 h. The mixture was cooled to 22 °C, evaporated and the residue partitioned between EtOAc and saturated aqueous Na_2CO_3-solution. The organic layers were dried over Na_2SO_4, filtered, evaporated and the residue was purified by flash column chromatography on silica gel using a mixture of n-heptane/EtOAc (5:2) to afford the title compound **11** (1.30 g, 79%) as a pale yellow solid: ^{1}H NMR (600 MHz, $CDCl_3$) δ ppm 8.59 (dd, *J*=6.6, 2.9 Hz, 1 H), 8.21 (ddd, *J*=9.0, 3.8, 3.0 Hz, 1 H), 7.20 (dd, *J*=10.6, 8.9 Hz, 1 H), 4.25–4.45 (2 H), 4.27 (ddd, *J*=23.2, 11.8, 3.8 Hz, 1 H), 4.06 (ddd, *J*=11.7, 10.4, 8.2 Hz, 1 H), 1.79 (t, *J*=2.3 Hz, 3 H). MS (ISP): *m/z* = 290.2

$[M+H]^+$. A small sample was recrystallized from EtOAc/n-heptane: m.p. 134-135 °C. Anal. ($C_{11}H_{10}F_3N_3O_3$) calcd C 45.68%, H 3.49%, N 14.53%; found C 45.63%, H 3.41%, N 14.65%.

(*R*)-4-(5-Amino-2-fluoro-phenyl)-5,5-difluoro-4-methyl-5,6-dihydro-4H-[1,3]oxazin-2-ylamine (13).[43] To a solution of (R)-5,5-difluoro-4-(2-fluoro-5-nitro-phenyl)-4-methyl-5,6-dihydro-4H-[1,3]oxazin-2-ylamine **11** (1.29 g, 4.47 mmol) in EtOH (35 mL) was added at 22 °C under an inert atmosphere palladium on carbon (10% Pd, 238 mg) and the mixture was stirred under a hydrogen atmosphere (balloon) at 22 °C for 1 h. The catalyst was filtered off, washed twice with EtOH, the solvent was removed under reduced pressure to give the crude title compound **15** (1.14 g, 98%) as a colorless foam which was used without further purification. ^{1}H NMR (600 MHz, $CDCl_3$) δ ppm 6.85 (dd, *J*=11.7, 8.6 Hz, 1 H), 6.79 (dd, *J*=6.5, 3.0 Hz, 1 H), 6.58 (ddd, *J*=8.6, 3.2, 3.1 Hz, 1 H), 4.10–4.90 (br s, 2 H), 4.10 (ddd, *J*=13.2, 11.5, 7.5 Hz, 1 H), 3.99 (ddd, *J*=18.2, 11.6, 5.9 Hz, 1 H), 3.55 (br s, 2 H), 1.75 (t, *J*=2.3 Hz, 3 H). MS (ISP): *m/z* = 260.1 $[M+H]^+$. A small sample was purified by flash column chromatography on silica gel using a mixture of dichloromethane/methanol (19:1) containing 1% of ammonium hydroxide, followed by crystallization from tert-butylmethyl ether: m.p. 122-123 °C. Anal. ($C_{11}H_{12}F_3N_3O$) calcd C 50.97%, H 4.67%, N 16.21%; found C 51.03%, H 4.52%, N 16.34%.

General Procedure for the synthesis of the amides 14a and 14d. To a solution of the carboxylic acid (0.23 mmol) in MeOH (5 mL) at 0 °C was added 4-(4,6-dimethoxy[1.3.5]triazin-2-yl)-4-methylmorpholinium chloride hydrate (DMTMM) (80 mg, 0.27 mmol). The colorless solution was stirred at 0 °C for 30 min, then a solution of (R)-4-(5-amino-2-fluoro-phenyl)-5,5-difluoro-4-methyl-5,6-dihydro-4H-[1,3]oxazin-2-ylamine (**13**) (54 mg, 0.21 mmol) in MeOH (5 mL) was added dropwise at 0 °C and the mixture was stirred at 22 °C for 20 h. The mixture was partitioned between aqueous Na_2CO_3-solution (1 M) and dichloromethane, the organic layers were washed with brine, dried over Na_2SO_4 and evaporated. The residue was purified by flash column chromatography on silica gel using a mixture of methanol/methylene chloride (0-10%) to give the pure amides **14a** and **14d**.

5-Chloro-pyridine-2-carboxylic acid [3-((*R*)-2-amino-5,5-difluoro-4-methyl-5,6-dihydro-4H-[1,3]oxazin-4-yl)-4-fluoro-phenyl]-amide (14a).[43] The condensation of **13** (110 mg, 0.42 mmol) and 5-

chloro-pyridine-2-carboxylic acid (67 mg, 0.42 mmol) yielded the title compound **14a** (122 mg, 72%) as a colorless solid: ^{1}H NMR (300 MHz, DMSO-d_6) δ ppm 10.70 (s, 1 H), 8.79 (d, *J*=2.0 Hz, 1 H), 8.13–8.22 (m, 2 H), 7.95 (dd, *J*=7.1, 2.6 Hz, 1 H), 7.83–7.91 (m, 1 H), 7.15 (dd, *J*=11.8, 8.8 Hz, 1 H), 4.29 (ddd, *J*=17.8, 12.0, 5.8 Hz, 1 H), 4.02 (ddd, *J*=17.8, 11.8, 5.8 Hz, 1 H), 3.30 (s, 2 H), 1.64 (s, 3 H). LC-HRMS: *m/z* 399.0839 [(M+H)$^+$ calcd for $C_{17}H_{15}ClF_3N_4O_2^+$, 399.0830]. MS (ISP): *m/z* = 399.2 [M+H]$^+$.

5-Cyano-pyridine-2-carboxylic acid [3-((*R*)-2-amino-5,5-difluoro-4-methyl-5,6-dihydro-4H-[1,3]oxazin-4-yl)-4-fluoro-phenyl]-amide (14d).[43] The condensation of **13** (80 mg, 0.31 mmol) and 5-cyano-pyridine-2-carboxylic acid (50 mg, 0.34 mmol) yielded the title compound **14d** (78 mg, 65%) as a colorless solid: ^{1}H NMR (600 MHz, DMSO-d_6) δ ppm 10.86 (s, 1 H), 9.20 (dd, *J*=2.1, 0.9 Hz, 1 H), 8.58 (dd, *J*=8.2, 2.1 Hz, 1 H), 8.28 (dd, *J*=8.2, 0.8 Hz, 1 H), 7.98 (dd, *J*=7.2, 2.8 Hz, 1 H), 7.88 (ddd, *J*=8.8, 3.8, 2.9 Hz, 1 H), 7.17 (dd, *J*=11.8, 8.8 Hz, 1 H), 5.91 (br s, 2 H), 4.30 (ddd, *J*=18.5, 11.9, 5.4 Hz, 1 H), 4.03 (ddd, *J*=17.4, 11.8, 5.7 Hz, 1 H), 1.65 (s, 3 H). LC-HRMS: *m/z* 390.1183 [(M+H)$^+$ calcd for $C_{18}H_{15}F_3N_5O_2^+$, 390.1172]. MS (ISP): *m/z* = 390.2 [M+H]$^+$. X-ray PDB accession code: 3ZMG.

3-Methyl-5-(trifluoromethyl)-4,5-dihydroisoxazole (76). To diethyl ether (640 mL) was added subsequently at -78 °C 3,3,3-trifluoroprop-1-ene (65.3 g, 680 mmol), nitroethane (30.0 g, 400 mmol), Et_3N (405 mg, 4 mmol) and phenyl isocyanate (97.2 g, 816 mmol), the solution was warmed to 22 °C and stirring was continued for 74 h. The suspension was filtered and the filtrate distilled from bulb to bulb at 50-60 °C/1.0 mbar to give a 9:1 mixture of the title compound **76** and its corresponding position isomer (37.3 g, 61%) as a pale yellow liquid. ^{1}H NMR (600 MHz, $CDCl_3$) δ ppm 4.80–4.87 (m, 1 H), 3.24 (ddq, *J*=17.8, 11.5, 1.0, 1.0, 1.0 Hz, 1 H), 3.08 (ddq, *J*=17.8, 5.8, 0.9, 0.9, 0.9 Hz, 1 H), 2.04 (t, *J*=1.1 Hz, 3 H). ^{1}H NMR signals of position isomer 3-methyl-4-(trifluoromethyl)-4,5-dihydroisoxazole: 4.44–4.53 (m, 2 H), 3.83–3.91 (m, 1 H), 2.12 (t, J=0.9 Hz, 3 H). MS: m/z = 153 [M]$^+$. Anal. ($C_5H_6F_3NO$) calcd C 39.22%, H 3.95%, N 9.15%; found C 39.27%, H 3.60%, N 9.34%.

(3S,5S)-3-(2-Fluoro-phenyl)-3-methyl-5-trifluoromethyl-isoxazolidine (79). To a stirred solution of 1-bromo-2-fluoro-benzene (**77**) (11.2 g, 64 mmol) in THF (50 mL) and toluene (140 mL) was added at -78 °C n-BuLi (1.6 M in hexane, 38 mL, 61 mmol) keeping the temperature below -70 °C and stirring

was continued at -78 °C for 1 h. To a solution of 3-methyl-5-(trifluoromethyl)-4,5-dihydroisoxazole (**76**) (4.68 g, 30.6 mmol) in toluene (330 mL) was added at -78 °C $BF_3{\cdot}Et_2O$ (8.68 g, 61.1 mmol) which was followed by the addition of the phenyl lithium reagent prepared above using an insulated cannula over 10 min keeping the temperature below -70 °C. The mixture was stirred at -78 °C for 1 h, quenched with saturated aqueous NH_4Cl and extracted with EtOAc. The organic layers were washed with brine, dried, evaporated and the residue was purified by flash column chromatography on silica gel using a mixture of n-heptane/EtOAc (50:1) to give the racemic title compound **79** (4.275 g, 56 %) as a pale yellow liquid. The racemate was resolved on a chiral HPLC column (Chiralpack AD) using n-heptane/EtOH (95:5) to give the desired (3S,5S)-3-(2-fluoro-phenyl)-3-methyl-5-trifluoromethyl-isoxazolidine (**79**) (1.719 g, 23%) as the slower eluting enantiomer with positive optical rotation and an *ee* >99.5%. ^{1}H NMR (300 MHz, $CDCl_3$) δ ppm 7.78 (td, *J*=8.0, 1.3 Hz, 1 H), 7.22–7.31 (m, 1 H), 7.14 (td, *J*=7.7, 1.2 Hz, 1 H), 7.05 (ddd, *J*=12.0, 8.1, 1.1 Hz, 1 H), 5.67 (s, 1 H), 4.27 (sxt, *J*=7.4 Hz, 1 H), 3.10 (ddd, *J*=13.4, 8.2, 1.0 Hz, 1 H), 2.37 (dd, *J*=13.3, 7.5 Hz, 1 H), 1.62 (s, 3 H). MS: m/z = 250.4 $[M+H]^+$. The relative and absolute configuration of the newly introduced stereogenic centers were confirmed by X-ray crystallographic analysis of the target compound **89** complexed with BACE1 (4J1F). (3R,5R)-3-(2-Fluoro-phenyl)-3-methyl-5-trifluoromethyl-isoxazolidine (1.738 g, 23%) was obtained as the faster eluting enantiomer with negative optical rotation and an *ee* >99.5%.

(2S,4S)-4-Amino-1,1,1-trifluoro-4-(2-fluorophenyl)pentan-2-ol (81). To a solution of (3S,5S)-3-(2-fluoro-phenyl)-3-methyl-5-trifluoromethyl-isoxazolidine (**79**) (1.50 g, 6.02 mmol) in EtOH (35 mL) was at 22°C ammonium formate (3.04 g. 48.2 mmol) and Pd/C (10%, 320 mg) and stirring of the mixture was continued at 22 °C for 4 h. The suspension was filtered, the filtrate evaporated and the residue was partitioned between EtOAc and saturated aqueous $NaHCO_3$ solution. The organic layer was dried and evaporated to give the crude title compound (1.50 g, 99%) as a colorless solid which was used without further purification. ^{1}H NMR (300 MHz, $CDCl_3$) δ ppm 7.45 (td, *J*=8.1, 1.8 Hz, 1 H), 7.28–7.37 (m, 1 H), 7.19 (td, *J*=7.5, 1.2 Hz, 1 H), 7.09 (ddd, *J*=12.6, 8.1, 1.3 Hz, 1 H), 3.61 (dqd, *J*=11.4, 6.7, 6.7, 6.7, 2.0 Hz, 1 H), 2.50 (dt, *J*=14.3, 1.6 Hz, 1 H), 1.75–2.75 (br, 2 H), 1.82 (dd, *J*=14.3, 11.5 Hz, 1 H),

1.69 (d, *J*=1.2 Hz, 3 H) (OH not detectable). MS: m/z = 252.2 $[M+H]^+$. A small sample was purified by flash column chromatography on silica gel using a mixture of n-heptane/EtOAc: m.p. 113-115 °C. Anal. ($C_{11}H_{13}F_4NO$) calcd C 52.59%, H 5.22%, N 5.58%; found C 52.49%, H 5.24%, N 5.73%.

(4S,6S)-4-(2-Fluorophenyl)-4-methyl-6-(trifluoromethyl)-5,6-dihydro-4H-1,3-oxazin-2-amine (83). To a solution of (2S,4S)-4-amino-1,1,1-trifluoro-4-(2-fluorophenyl)pentan-2-ol (**81**) (1.834 g, 7.30 mmol) in EtOH (38 mL) was added a solution of Br-CN (5 M in CH_3CN, 2.2 mL, 11.0 mmol) and the mixture was stirred in a sealed tube at 85 °C for 15 h. The mixture was evaporated and the residue partitioned between EtOAc and saturated aqueous Na_2CO_3 solution, the organic layer was dried, evaporated and the residue was purified by chromatography (silica-NH_2) using a mixture of n-heptane/EtOAc (5:1 to 0:1) to afford the title compound **83** (817 mg, 41%) as a colorless oil. ^{1}H NMR (600 MHz, $CDCl_3$) δ ppm 7.38 (td, *J*=8.1, 1.9 Hz, 1 H), 7.24–7.29 (m, 1 H), 7.13 (td, *J*=7.6, 1.3 Hz, 1 H), 7.04 (ddd, *J*=12.4, 8.1, 1.3 Hz, 1 H), 4.35 (br s, 2 H), 3.97 (dqd, *J*=12.4, 6.0, 6.0, 6.0, 2.8 Hz, 1 H), 2.77 (dd, *J*=13.6, 2.8 Hz, 1 H), 1.86 (dd, *J*=13.6, 12.6 Hz, 1 H), 1.63 (d, *J*=1.3 Hz, 3 H). MS: m/z = 277.1 $[M+H]^+$. A small sample was subjected again to flash column chromatography on silica-NH_2 gel using a mixture of n-heptane/EtOAc: Anal. ($C_{12}H_{12}F_4N_2O$) calcd C 52.18%, H 4.38%, N 10.14%; found C 52.04%, H 4.14%, N 10.05%.

(4S,6S)-4-(2-Fluoro-5-nitrophenyl)-4-methyl-6-(trifluoromethyl)-5,6-dihydro-4H-1,3-oxazin-2-amine (85). To concentrated sulfuric acid (11 mL) was added portion wise (4S,6S)-4-(2-fluorophenyl)-4-methyl-6-(trifluoromethyl)-5,6-dihydro-4H-1,3-oxazin-2-amine (**83**) (760 mg, 2.75 mmol) at 22 °C, the solution obtained was cooled to 0 °C and treated with red fuming HNO_3 (0.17 mL, 3.85 mmol) over 20 min and stirring was continued at 0 °C for 30 min. The reaction mixture was slowly added to crushed ice/water (150 mL), the pH was adjusted to 10 using NaOH, the aqueous layer was extracted with EtOAc, the organic layer was dried, evaporated and the residue was chromatographed on silica gel using a mixture of n-heptane/EtOAc (3:1) to afford the title compound **85** (800 mg, 91%) as a pale yellow oil. ^{1}H NMR (300 MHz, $CDCl_3$) δ ppm 8.37 (dd, *J*=7.0, 2.9 Hz, 1 H), 8.19 (ddd, *J*=8.9, 4.0, 3.0 Hz, 1 H),

7.21 (dd, *J*=10.7, 8.9 Hz, 1 H), 4.31 (br s, 2 H), 3.87–4.01 (m, 1 H), 2.78 (dd, *J*=13.8, 2.7 Hz, 1 H), 1.95 (dd, *J*=13.8, 12.8 Hz, 1 H), 1.64 (d, *J*=1.2 Hz, 3 H). MS: m/z = 322.5 $[M+H]^+$.

(4S,6S)-4-(5-Amino-2-fluorophenyl)-4-methyl-6-(trifluoromethyl)-5,6-dihydro-4H-1,3-oxazin-2-amine (87). A suspension of (4S,6S)-4-(2-fluoro-5-nitrophenyl)-4-methyl-6-(trifluoromethyl)-5,6-dihydro-4H-1,3-oxazin-2-amine (**85**) (765 mg, 2.38 mmol) in EtOH (45 mL) and Et_3N (0.33 mL, 2.38 mmol) was treated with Pd/C (10%, 127 mg) and the mixture was hydrogenated at atmospheric pressure and 22 °C for 3 h. The mixture was filtered and the filtrate evaporated to give the crude title compound **87** (680 mg, 98%) as a colorless foam which was used without further purification. ^{1}H NMR (300 MHz, $CDCl_3$) δ ppm 6.83 (dd, *J*=11.7, 8.5 Hz, 1 H), 6.67 (dd, *J*=6.9, 2.8 Hz, 1 H), 6.52 (ddd, *J*=8.5, 3.0, 3.0 Hz, 1 H), 4.04 (dqd, *J*=12.3, 6.0, 6.0, 6.0, 2.8 Hz, 1 H), 3.90–4.60 (br s, 2 H), 3.57 (br s, 2 H), 2.76 (dd, *J*=13.5, 2.8 Hz, 1 H), 1.81 (dd, *J*=13.4, 12.6 Hz, 1 H), 1.60 (d, *J*=1.2 Hz, 3 H). MS: m/z = 292.5 $[M+H]^+$. Anal. ($C_{12}H_{13}F_4N_3O$) calcd C 49.49%, H 4.50%, N 14.43%; found C 49.25%, H 4.51%, N 14.15%.

N-(3-((4S,6S)-2-amino-4-methyl-6-(trifluoromethyl)-5,6-dihydro-4H-1,3-oxazin-4-yl)-4-fluorophenyl)-5-cyanopicolinamide (89). The coupling of (4S,6S)-4-(5-amino-2-fluorophenyl)-4-methyl-6-(trifluoromethyl)-5,6-dihydro-4H-1,3-oxazin-2-amine (**87**) and 5-cyano-pyridine-2-carboxylic acid (**65**), carried out according to the general procedure for **14a** and **14d**, yielded a crude material which was purified by chromatography (silica-NH_2) using a mixture of n-heptane/EtOAc (1:1) to give the title compound **89** (69% yield) as a colorless solid: ^{1}H NMR (300 MHz, $CDCl_3$) δ ppm 9.84 (s, 1 H), 8.89 (dd, *J*=2.0, 0.8 Hz, 1 H), 8.43 (dd, *J*=8.1, 0.8 Hz, 1 H), 8.20 (dd, *J*=8.3, 2.0 Hz, 1 H), 7.99 (ddd, *J*=8.7, 4.1, 2.9 Hz, 1 H), 7.48 (dd, *J*=7.1, 2.8 Hz, 1 H), 7.11 (dd, *J*=11.4, 8.8 Hz, 1 H), 4.24 (br s, 2 H), 4.03 (dqd, *J*=12.2, 6.0, 6.0, 6.0, 2.6 Hz, 1 H), 2.81 (dd, *J*=13.7, 2.6 Hz, 1 H), 1.89 (dd, *J*=13.6, 12.8 Hz, 1 H), 1.64 (d, *J*=1.0 Hz, 3 H). LC-HRMS *m/z* 422.1243 [$(M+H)^+$ calcd for $C_{19}H_{16}F_4N_5O_2^+$, 422.1235]. MS: m/z = 422.5 $[M+H]^+$. X-ray PDB accession code: 4J1F.

BACE1 & BACE2 Enzyme Assay. Enzyme inhibition assays were performed in 384-well microtiter plates (black with clear bottom, non-binding surface from Corning, Cat. No.: 3655) in a final volume of

51 µl. Test compounds dissolved in DMSO at a concentration of 10mM were serially diluted in DMSO (15 concentrations, 1/3 dilution steps, final concentration range: 200-0.0004 µM). 1 µl of diluted compounds were mixed with 40 µl of enzyme on an H&P Teleshaker for 4 min. After addition of the MR121-labelled substrate, the plates were again strongly shaken for 2 min. The enzymatic reaction was followed by reading the fluorescence emission on a plate: vision reader (Perkin-Elmer) (excitation wavelength: 630 nm; emission: 695 nm) for at least 30 min in a kinetic measurement detecting an increase of MR121 fluorescence following the cutting of the quenched substrate. The slope in the linear range of the kinetic was calculated and the IC_{50} of the test compounds were determined using a four parameter Hill equation for curve fitting on the calculated %-inhibition values referenced to wells without enzyme and wells with enzyme but no test compound respectively. BACE1 enzyme used in the assay was prepared and purified as described.[58] The preparation of BACE2 was carried out following exactly the known protocol.[46] BACE1/2 assay: The final enzyme concentration in the assay was 30 and 125 nM respectively. The assay buffer was 100 mM sodium acetate, 20 mM EDTA, 0.05 % BSA, pH4.0. The substrate peptide was of sequence WSEVNLDAEFRC-MR121 and used at a final concentration of 300 nM.

Cathepsin D Enzyme Assay. Cathespsin D from human liver was purchased from Calbiochem (Cat. No.: 219401) and used at a final concentration of 200 nM. The assay buffer was 100 mM sodium acetate at pH 5.5 with 0.05% BSA. The labeled substrate peptide was of sequence WTSVLMAAPC-MR121. (Measurement time > 60 min).

Cathepsin E Enzyme Assay. Recombinant human Cathepsin E was purchased from R&D-Systems (Cat. No.: 1294-AS) and used at a final concentration of 0.01 nM. The assay buffer was 100 mM sodium acetate at pH 4.5 with 0.05% BSA. The labeled substrate was of sequence MR121-CKLVFFAEDW.

Renin Enzyme Assay. Renin was purchased from Anaspec (Cat. No.: 72041) and used at a final concentration of 5 nM. The assay buffer was 50 mM MES at pH6.2 with 0.5% BSA and 2mM EDTA. The substrate peptide was of sequence WIPHPFHLVIHTC-MR121.

Pepsin Enzyme Assay. Pepsin from Porcine stomach mucosa was purchased from Calbiochem (Cat. No.: 516360) and used at a final concentration of 8 nM. The assay buffer was 100 mM sodium acetate at pH 4.0 with 0.05% BSA and the substrate was the same as for Cathepsin D. All substrate peptides were prepared and purified by Biosyntan, Berlin, Germany and purchased as lyophilized powders. After reconstitution in DMSO small aliquots were kept at -20 °C.

Cell-Based Assay. HEK293 cells transfected with wild-type human APP cDNA were seeded in 96 well Microtiter plates in cell culture medium (Iscove's, plus 10% (v/v) fetal bovine serum, penicillin/streptomycin) to about 80% confluency and the compounds were added at a 3× concentration in 1/3 volume of culture medium (final DMSO concentration was kept at 1% v/v). After 18-20 h incubation at 37 °C and 5% CO_2 in a humidified incubator, the culture supernatants were harvested for the determination of Aβ40 concentrations by AlphaLISA technique using PerkinElmer Human Amyloid beta 1-40 kit (Aβ1-40, high specificity, Cat# AL275 C/F). In a PerkinElmer OptiPlate -384 (Cat# 6007290), 6 μL of culture supernatants were added to 2 μL of AlphaLISA Anti hu Aβ acceptor beads (50μg/ml), 5 nM Biotinylated Antibody Anti Aβ1-40, 1× AlphaLISA HiBlock buffer solution and incubated for 1 h at room temperature. Then 16 μL of a Streptavidin Donor beads (250ng/ml in 1× AlphaLISA solution) were added and the plate was incubated for 30 min at room temperature. Light Emission at 615 nm was then recorded on an EnVision-2104 Multilabel Reader. Levels of Aβ40 in the culture supernatants were calculated as percentage of maximum signal (cells treated with 1% DMSO without inhibitor). The IC_{50} values were calculated using the Excel XLfit software.

P-gp assay. Bidirectional transport was examined in LLC-PK1 cells (Lewis-lung cancer porcine kidney 1 1, ATCC #CL-101) stably expressing human MDR1. The cell lines were obtained from Dr. Alfred Schinkel, The Netherlands Cancer Institute (Amsterdam, The Netherlands) and used under a license agreement. Both cell lines were cultured on semi-permeable insert plates (Costar, surface area 0.33 cm^2, pore size 3.0 μm) and transport experiments were performed on day 4 after seeding using medium without phenol red. Bidirectional transport was assessed in triplicate inserts with or without

inhibitor (elacridar, 1 μM) and the cell monolayer integrity was assessed via the permeability of lucifer yellow (10 μM). Before each assay, the culture medium in the receiver compartment was replaced with fresh medium. Bidirectional transport was then initiated by the addition of medium consisting of test compound (1 μM) and lucifer yellow, to the donor compartments. The plates were incubated for 3.5 h at 37 °C, 5% CO_2 and air-saturated humidity. At the end of incubation, samples were taken from the donor and the receiver compartments and the levels of each compound were determined either by LC-MS/MS or scintillation counting. Lucifer yellow in the receiver samples was quantified using a fluorescence-based plate reader set at excitation and emission wavelengths of 430 nm and 535 nm, respectively. Experiments showing lucifer yellow permeation superior to 1%/h were rejected. The apparent permeability coefficient (Papp) was calculated using the following equation: $Papp = 1/(A \cdot C_0)$. (dQ/dt), where dQ/dt is the amount of compound transported over time, A is the surface area of the transwell, and C_0 is the initial concentration of the test compound. Mean Papp value and standard deviation were calculated from triplicate inserts. Active efflux by MDR1 was assessed by determining the vectorial transport or efflux ratio (ER), calculated from the basolateral-to-apical Papp divided by the apical-to-basolateral Papp. Digoxin was included in each experiment as a positive control.

HERG inhibition. HERG inhibition was tested as described.[59]

Protein crystallography. X-ray crystal structures of BACE1 and BACE2 were determined as described by Kuglstatter et al.[60] and Ruf et al.[48]

Pharmacokinetic experiments in mice and rats. Animals and Housing Conditions. Animals were maintained in a 12:12 h light:dark cycle, with lights starting at 6 am, and experiments were conducted during the light phase. Animal housing and experimental procedures were in line with ethical and legal guidelines, and were authorized by local veterinary authorities.

Experiment. Compound **89** was administered to female C57Bl/6NJ mice. At indicated time points plasma and brain samples were quenched with organic solvent. (1volume of sample + 3volumes of acetonitrile/methanol, 1:1 (v/V) containing an internal standard). After centrifugation for min at 4000 g, the supernatant was diluted with one volume of aqueous 10 mM ammonium acetate at pH 3. Samples

were then directly injected onto an LC-MS/MS system to quantify compound concentrations against a calibration curve using analyte specific transitions. Pharmacokinetic studies in rats were conducted accordingly using the following formulations: PO microsuspension in gelatine/NaCl (7.5% / 0.62% in water) at 1.25 mg 89/mL; IV 0.5 mg 89 / mL 0.9% NaCl in water/NMP (30/70).

Inhibition of Aβ40 in brain of wild-type mice. Animals and Housing Conditions. Animals were maintained in a 12:12 h light:dark cycle, with lights starting at 6 am, and experiments were conducted during the light phase. Animal housing and experimental procedures were in line with ethical and legal guidelines, and were authorized by local veterinary authorities.

Experiment. Female C57Bl/6J mice were treated with different doses of the compounds, 3-4 animals per treatment group. The test compound was dissolved in 5% EtOH, 10% Solutol and was applied per os at 10 mL/kg. After 4h the animals were sacrificed and brain and plasma were collected. The brain was cut into halves and immediately frozen on dry ice. Brain was used for measurement of Aβ40 and plasma was used for determination of compound exposure. The method for Aβ40 determination in brain lysates followed the known procedure.[61] Brain tissue was homogenized in 2% DEA buffer in a Roche MagnaLyser (20", 4000 rpm) and subsequently centrifuged for 1 h at 100'000g. DEA was reduced to 0.2% in 50 mM NaCl and one half of the DEA lysate was passed over an Oasis Solid Phase extraction plate (Waters; Cat.Nr. 186000679) which had been activated with MeOH and equilibrated in dH_2O (1ml each). After washes in 10% and 30% MeOH (1 ml each) the Aβ-peptides were eluted in 0.8 ml 2% NH_4OH in 90% MeOH. The eluate was dried over a N_2 flow and the dried sample was reconstituted in 30 µl AlphaLISA assay buffer. Aβ40 was determined by an AlphaLISA assay (Perkin Elmer). In a white 96well half-area microplate (Perkin Elmer Cat.Nr. 6005561), 20 µl of the reconstituted sample were mixed with 5 µl biotinylated BAP-24 (specific for C-terminus of $Aβ40^{62}$), stock = 4.4 mg/ml, f.c.5.5 µg/ml) and 5 µl 252Q6 acceptor beads (252Q6 antibody, Invitrogen AMB0062) had been previously conjugated with AlphaLISA Acceptor beads (Perkin Elmer Cat.Nr.6772002); final dilution 1:500). The mix was incubated for 1h at RT in the dark. Then 20 µl Streptavin-coated Donor Beads (Perkin Elmer

Cat. Nr. 6760002, final dilution 1:125) were added and this final mix was incubated in the dark for another 30 min at RT before RFU was measured in an AlphaScreen Reader(Perkin Elmer Envision 2104).

Inhibition of CSF Aβ40 in wild-type rats. Animals and Housing Conditions. Animals were maintained in a 12:12 h light:dark cycle, with lights starting at 6 am, and experiments were conducted during the light phase. Animal housing and experimental procedures were in line with ethical and legal guidelines, and were authorized by local veterinary authorities.

Experiment. In this *in vivo* model we followed the kinetics of changes in rat CSF Aβ40 in an acute treatment study. For this purpose male rats (Wistar) were prepared with a cannula inserted into the Cisterna magna.[57] Approximately 1 week after surgery 2-3 animals were treated with one dose of the test compound by gavage (compound prepared in 10% solutol, 5% ethanol and 85% water, 4 ml/kg). CSF was drawn at 2 and 1 hour before compound application and then at different time points post-application, the volume of CSF withdrawn at each time-point was about 10 µl. For the determination of Aβ-peptide in the rat CSF a commercial ELISA kit specific for Aβ40 was used according to the protocol of the manufacturer (WAKO, Cat no. 294-64701, human/rat β-amyloid 40). Because of inter-animal differences in baseline Aβ40 level in CSF the pre-treatment samples were used to define the 100% Aβ40 level for each individual animal and the subsequent post-treatment values were expressed as percentage of this control value.

ASSOCIATED CONTENT

Supporting Information. Preparation details and analytical data for compounds **1a-b, 14b-c, 14e-v, 66–70, 88, 109–113**. LogD, pKa determinations, stability in mouse microsomes, inhibition of CYP_{450s} and time dependent inhibition of CYP_{450} 3A4. This material is available free of charge via the internet at http://pubs.acs.org.

Accession Codes. Crystal structure coordinates and structure factors have been deposited to the PDB with the accession numbers 4J0P (**1b**), 3ZMG (**14d**), 4J0T (**14i**), 4J0V (**66**), 4J0Y (**67**), 4J0Z (**68**), 4J17 (**69**), 4J1C (**70**), 4J1E (**88**), 4J1F (**89**), 4J1H (**109**), 4J1I (**110**) and 4J1K (**111**). The structure of BACE2 in complex with **14i** has been deposited with the accession number 3ZLQ.

AUTHOR INFORMATION

Corresponding Author. *Dr. Hans Hilpert, F. Hoffmann-La Roche Ltd, Bldg. 92/2.88, CH-4070 Basel, Switzerland. Phone: +41 61 688 72 64. E-mail: hans.hilpert@roche.com.

Notes: The authors declare no competing financial interest.

ACKNOWLEDGEMENTS

We thank A. Fettes, R. Halm, C. Kuratli and H.P. Marty for synthesis support, D. Zimmerli for separations on chiral HPLC, J. Schneider for NMR spectroscopy, C. Bartelmus for mass spectroscopy, L. Polonchuk for hERG data, S. Bendels for logP calculations, M. Stihle and D. Schlatter for protein crystallization and production, and N. Kratochwil, A. Pähler, A. Poirier, V. Starke and K. Youdim for DMPK support.

ABBREVIATIONS USED

HERG, human ether-à-go-go related gene; DCM, dichloromethane; Deoxo-Fluor®, bis(2-methoxyethyl)aminosulfur trifluoride; DIBAH, diisobutylaluminumhydride; DMF, N,N-dimethylformamide, DMSO, dimethyl sulfoxide; DMTMM, 4-(4,6-Dimethoxy[1.3.5]triazin-2-yl)-4-methylmorpholinium chloride hydrate; EtOAc, ethyl acetate; EtOH, ethanol; MeOH, methanol; TBME, tert-butylmethylether; TEA, triethylamine; TFA, trifluoro-acetic acid; T3P®, (2,4,6-tripropyl-1,3,5,2,4,6-trioxatriphosphorinane-2,4,6-trioxide; TBAF, tetrabutylammonium fluoride; THF, tetrahydrofuran.

REFERENCES

1. Jakob-Roetne, R.; Jacobsen, H. Alzheimer's Disease: From Pathology to Therapeutic Approaches. *Angew. Chem., Int. Ed.* **2009,** *48*, 3030-3059.

2. Hardy, J. A.; Higgins, G. A. Alzheimer's disease: the amyloid cascade hypothesis. *Science* **1992,** *256*, 184-185.

3. Selkoe, D. J. Cell biology of the amyloid β-protein precursor and the mechanism of Alzheimer's disease. *Annu. Rev. Cell Biol.* **1994,** *10*, 373-403.

4. Selkoe, D. J. The molecular pathology of Alzheimer's disease. *Neuron* **1991,** *6*, 487-498.

5. Selkoe, D. J. Toward a comprehensive theory for Alzheimer's disease. Hypothesis: Alzheimer's disease is caused by the cerebral accumulation and cytotoxicity of amyloid β-protein. *Ann. N. Y. Acad. Sci.* **2000,** *924*, 17-25.

6. Citron, M. Alzheimer's disease: strategies for disease modification. *Nat. Rev. Drug Discovery* **2010,** *9*, 387-398.

7. Vassar, R. The β-secretase, BACE. A prime drug target for Alzheimer's disease. *J. Mol. Neurosci.* **2001,** *17*, 157-170.

8. Cole, S. L.; Vassar, R. BACE1 structure and function in health and Alzheimer's disease. *Curr. Alzheimer Res.* **2008,** *5*, 100-120.

9. Cai, H.; Wang, Y.; McCarthy, D.; Wen, H.; Borchelt, D. R.; Price, D. L.; Wong, P. C. BACE1 is the major beta-secretase for generation of Abeta peptides by neurons. *Nat Neurosci* **2001,** *4*, 233-234.

10. Luo, Y.; Bolon, B.; Kahn, S.; Bennett, B. D.; Babu-Khan, S.; Denis, P.; Fan, W.; Kha, H.; Zhang, J.; Gong, Y.; Martin, L.; Louis, J.-C.; Yan, Q.; Richards, W. G.; Citron, M.; Vassar, R. Mice deficient in BACE1, the Alzheimer's β-secretase, have normal phenotype and abolished β-amyloid generation. *Nat. Neurosci.* **2001,** *4*, 231-232.

11. McConlogue, L.; Buttini, M.; Anderson, J. P.; Brigham, E. F.; Chen, K. S.; Freedman, S. B.; Games, D.; Johnson-Wood, K.; Lee, M.; Zeller, M.; Liu, W.; Motter, R.; Sinha, S. Partial reduction of BACE1 has dramatic effects on Alzheimer plaque and synaptic pathology in APP transgenic mice. *J. Biol. Chem.* **2007,** *282*, 26326-26334.

12. Rabe, S.; Reichwald, J.; Ammaturo, D.; de, S. B.; Saftig, P.; Neumann, U.; Staufenbiel, M. The Swedish APP mutation alters the effect of genetically reduced BACE1 expression on the APP processing. *J Neurochem* **2011,** *119*, 231-239.

13. Hu, X.; Hicks, C. W.; He, W.; Wong, P.; Macklin, W. B.; Trapp, B. D.; Yan, R. Bace1 modulates myelination in the central and peripheral nervous system. *Nat. Neurosci.* **2006,** *9*, 1520-1525.

14. Willem, M.; Garratt, A. N.; Novak, B.; Citron, M.; Kaufmann, S.; Rittger, A.; DeStrooper, B.; Saftig, P.; Birchmeier, C.; Haass, C. Control of Peripheral Nerve Myelination by the β-Secretase BACE1. *Science (Washington, DC, U. S.)* **2006,** *314*, 664-666.

15. Esterhazy, D.; Stuetzer, I.; Wang, H.; Rechsteiner, M. P.; Beauchamp, J.; Doebeli, H.; Hilpert, H.; Matile, H.; Prummer, M.; Schmidt, A.; Lieske, N.; Boehm, B.; Marselli, L.; Bosco, D.; Kerr-Conte, J.; Aebersold, R.; Spinas, G. A.; Moch, H.; Migliorini, C.; Stoffel, M. Bace2 Is a β Cell-Enriched Protease that Regulates Pancreatic β Cell Function and Mass. *Cell Metab.* **2011,** *14*, 365-377.

16. Sinha, S.; Anderson, J. P.; Barbour, R.; Basi, G. S.; Caccavello, R.; Davis, D.; Doan, M.; Dovey, H. F.; Frigon, N.; Hong, J.; Jacobson-Croak, K.; Jewett, N.; Keim, P.; Knops, J.; Lieberburg, I.; Power, M.; Tan, H.; Tatsuno, G.; Tung, J.; Schenk, D.; Seubert, P.; Suomensaari, S. M.; Wang, S.; Walker, D.; Zhao, J.; McConlogue, L.; John, V. Purification and cloning of amyloid precursor protein β-secretase from human brain. *Nature (London)* **1999,** *402*, 537-540.

17. Vassar, R.; Bennett, B. D.; Babu-Khan, S.; Kahn, S.; Mendiaz, E. A.; Denis, P.; Teplow, D. B.; Ross, S.; Amarante, P.; Loeloff, R.; Luo, Y.; Fisher, S.; Fuller, J.; Edenson, S.; Lile, J.; Jarosinski, M. A.; Biere, A. L.; Curran, E.; Burgess, T.; Louis, J.-C.; Collins, F.; Treanor, J.; Rogers, G.; Citron, M. β-Secretase cleavage of Alzheimer's amyloid precursor protein by the transmembrane aspartic protease BACE. *Science (Washington, D. C.)* **1999,** *286*, 735-741.

18. Yan, R.; Bienkowski, M. J.; Shuck, M. E.; Miao, H.; Tory, M. C.; Pauley, A. M.; Brashler, J. R.; Stratman, N. C.; Mathews, W. R.; Buhl, A. E.; Carter, D. B.; Tomasselli, A. G.; Parodi, L. A.; Heinrikson, R. L.; Gurney, M. E. Membrane-anchored aspartyl protease with Alzheimer's disease β-secretase activity. *Nature (London)* **1999,** *402*, 533-537.

19. Lin, X.; Koelsch, G.; Wu, S.; Downs, D.; Dashti, A.; Tang, J. Human aspartic protease memapsin 2 cleaves the β-secretase site of β-amyloid precursor protein. *Proc. Natl. Acad. Sci. U. S. A.* **2000,** *97*, 1456-1460.

20. Hussain, I.; Powell, D.; Howlett, D. R.; Tew, D. G.; Meek, T. D.; Chapman, C.; Gloger, I. S.; Murphy, K. E.; Southan, C. D.; Ryan, D. M.; Smith, T. S.; Simmons, D. L.; Walsh, F. S.; Dingwall, C.; Christie, G. Identification of a Novel Aspartic Protease (Asp 2) as β-Secretase. *Mol. Cell. Neurosci.* **1999,** *14*, 419-427.

21. Probst, G.; Xu, Y.-z. Small-molecule BACE1 inhibitors: a patent literature review (2006 - 2011). *Expert Opin. Ther. Pat.* **2012,** *22*, 511-540.

22. Cohen, N.; Banner, B. L. Synthesis of 2-amino-5,6-dihydro-4H-1,3-thiazines and related compounds by acid catalyzed cyclization of allylic isothiuronium salts. *J. Heterocycl. Chem.* **1977,** *14*, 717-723.

23. Kobayashi, N.; Ueda, K.; Itoh, N.; Suzuki, S.; Sakaguchi, G.; Kato, A.; Yukimasa, A.; Hori, A.; Koriyama, Y.; Haraguchi, H.; Yasui, K.; Kanda, Y. Preparation of 2-aminodihydrothiazine derivatives as β-secretase inhibitors. WO2007049532A1, 2007.

24. Suzuki, Y.; Motoki, T.; Kaneko, T.; Takaishi, M.; Ishida, T.; Takeda, K.; Kita, Y.; Yamamoto, N.; Khan, A.; Dimopoulos, P. Preparation of condensed aminodihydrothiazine derivatives as inhibitors of β-site APP-cleaving enzyme 1 (BACE1). WO2009091016A1, 2009.

25. Audia, J. E.; Mergott, D. J.; Sheehan, S. M.; Watson, B. M. Preparation of aminodihydrothiazine derivatives for use as BACE inhibitors. WO2009134617A1, 2009.

26. Chen, J. J.; Zhong, W.; Yang, B.; Qian, W.; Lopez, P.; White, R.; Weiss, M.; Judd, T.; Powers, T.; Cheng, Y.; Dineen, T.; Epstein, O.; Low, J.; Marx, I.; Minatti, A. E.; Paras, N. A.; Potashman, M.

Aminodihydrooxazine and aminodihydrothiazine spiro compounds as beta-secretase modulators and their their preparation and medical use. WO2011115928A1, 2011.

27. Clark, C. T.; Cook, A.; Gunawardana, I. W.; Hunt, K. W.; Kallan, N. C.; Siu, M.; Thomas, A. A.; Volgraf, M. Spirotetrahydronaphthalene derivatives as β-secretase inhibitors and their preparation and use for the treatment of neurodegenerative diseases. WO2011123674A1, 2011.

28. May, P. C.; Dean, R. A.; Lowe, S. L.; Martenyi, F.; Sheehan, S. M.; Boggs, L. N.; Monk, S. A.; Mathes, B. M.; Mergott, D. J.; Watson, B. M.; Stout, S. L.; Timm, D. E.; LaBell, E. S.; Gonzales, C. R.; Nakano, M.; Jhee, S. S.; Yen, M.; Ereshefsky, L.; Lindstrom, T. D.; Calligaro, D. O.; Cocke, P. J.; Hall, D. G.; Friedrich, S.; Citron, M.; Audia, J. E. Robust central reduction of amyloid-β in humans with an orally available, non-peptidic β-secretase inhibitor. *J. Neurosci.* **2011,** *31*, 16507-16516.

29. Woltering, T. J.; Wostl, W.; Hilpert, H.; Rogers-Evans, M.; Pinard, E.; Mayweg, A.; Banner, D. W.; Benz, J.; Narquizian, R.; Travagli, M.; Power, E.; Pollastrini, M.; Marconi, G.; Gabellieri, E.; Guba, W.; Mauser, H.; Andreini, M.; Jacobsen, H. BACE1 Inhibitors: A Head Group Scan on a Series of Amides. Submitted to *Bioorg. Med. Chem. Lett.*

30. Tang, T. P.; Ellman, J. A. The tert-Butanesulfinyl Group: An Ideal Chiral Directing Group and Boc-Surrogate for the Asymmetric Synthesis and Applications of β-Amino Acids. *J. Org. Chem.* **1999,** *64*, 12-13.

31. Sorochinsky, A.; Voloshin, N.; Markovsky, A.; Belik, M.; Yasuda, N.; Uekusa, H.; Ono, T.; Berbasov, D. O.; Soloshonok, V. A. Convenient Asymmetric Synthesis of β-Substituted α,α-Difluoro-β-amino Acids via Reformatskii Reaction between Davis' N-Sulfinylimines and Ethyl Bromodifluoroacetate. *J. Org. Chem.* **2003,** *68*, 7448-7454.

32. Tamura, Y.; Suzuki, S.; Tada, Y.; Yonezawa, S.; Fujikoshi, C.; Matsumoto, S.; Kooriyama, Y.; Ueno, T. Preparation of aminodihydrothiazine derivatives as BACE1 inhibitors. WO2008133274A1, 2008.

33. Masui, M.; Anan, K. Aminothiazine or aminooxazine derivative having amino linker for treatment of Alzheimer disease. WO2011058763A1, 2011.

34. Kunishima, M.; Morita, J.; Kawachi, C.; Iwasaki, F.; Terao, K.; Tani, S. Esterification of carboxylic acids with alcohols by 4-(4,6-dimethoxy-1,3,5-triazin-2-yl)-4-methylmorpholinium chloride (DMTMM). *Synlett* **1999**, 1255-1256.

35. Jaeger, V.; Muller, I.; Schohe, R.; Frey, M.; Ehrler, R.; Hafele, B.; Schroter, D. Syntheses via isoxazolines. Part 18. Old concepts and recent results on stereoselection at isoxazoline ring and adjacent centers. *Lect. Heterocycl. Chem.* **1985,** *8*, 79-98.

36. Banner, D.; Hilpert, H.; Mauser, H.; Mayweg, A. V.; Rogers-Evans, M. Preparation of oxazine derivatives as BACE2 inhibitors for treatment of diabetes. WO2011070029A1, 2011.

37. Masui, M.; Hori, A. Preparation of 2-amino-4-(aryl or heterocyclyl)-1,3-oxazine derivatives as β-secretase (BACE1) inhibitors. WO2011071135A1, 2011.

38. Ellard, J. M.; Farthing, C. N.; Hall, A. Preparation of fused aminodihydrooxazine derivatives as β-amyloid inhibitors and useful in the treatment of neurodegenerative disease caused by Aβ in particular Alzheimer-type dementia. WO2011009898A1, 2011.

39. Price, D. A.; Blagg, J.; Jones, L.; Greene, N.; Wager, T. Physicochemical drug properties associated with in vivo toxicological outcomes: a review. *Expert Opin. Drug Metab. Toxicol.* **2009,** *5*, 921-931.

40. Peters, J.-U.; Schnider, P.; Mattei, P.; Kansy, M. Pharmacological Promiscuity: Dependence on Compound Properties and Target Specificity in a Set of Recent Roche Compounds. *ChemMedChem* **2009,** *4*, 680-686.

41. Peters, J.-U.; Hert, J.; Bissantz, C.; Hillebrecht, A.; Gerebtzoff, G.; Bendels, S.; Tillier, F.; Migeon, J.; Fischer, H.; Guba, W.; Kansy, M. Can we discover pharmacological promiscuity early in the drug discovery process? *Drug Discov Today* **2012,** *17*, 325-335.

42. Mueller, K.; Faeh, C.; Diederich, F. Fluorine in Pharmaceuticals: Looking Beyond Intuition. *Science (Washington, DC, U. S.)* **2007,** *317*, 1881-1886.

43. Banner, D.; Guba, W.; Hilpert, H.; Mauser, H.; Mayweg, A. V.; Narquizian, R.; Pinard, E.; Power, E.; Rogers-Evans, M.; Woltering, T.; Wostl, W. Preparation of 2-amino-5,5-difluoro-5,6-dihydro-4H-oxazine derivatives as BACE1 and/or BACE2 inhibitors. WO2011069934A1, 2011.

44. Patel, S.; Vuillard, L.; Cleasby, A.; Murray, C. W.; Yon, J. Apo and Inhibitor Complex Structures of BACE (β-secretase). *J. Mol. Biol.* **2004,** *343*, 407-416.

45. Stauffer, S. R.; Stanton, M. G.; Gregro, A. R.; Steinbeiser, M. A.; Shaffer, J. R.; Nantermet, P. G.; Barrow, J. C.; Rittle, K. E.; Collusi, D.; Espeseth, A. S.; Lai, M.-T.; Pietrak, B. L.; Holloway, M. K.; McGaughey, G. B.; Munshi, S. K.; Hochman, J. H.; Simon, A. J.; Selnick, H. G.; Graham, S. L.; Vacca, J. P. Discovery and SAR of isonicotinamide BACE-1 inhibitors that bind β-secretase in a N-terminal 10s-loop down conformation. *Bioorg. Med. Chem. Lett.* **2007,** *17*, 1788-1792.

46. Ostermann, N.; Eder, J.; Eidhoff, U.; Zink, F.; Hassiepen, U.; Worpenberg, S.; Maibaum, J.; Simic, O.; Hommel, U.; Gerhartz, B. Crystal Structure of Human BACE2 in Complex with a Hydroxyethylamine Transition-state Inhibitor. *J. Mol. Biol.* **2006,** *355*, 249-261.

47. Xu, Y.; Li, M.-j.; Greenblatt, H.; Chen, W.; Paz, A.; Dym, O.; Peleg, Y.; Chen, T.; Shen, X.; He, J.; Jiang, H.; Silman, I.; Sussman, J. L. Flexibility of the flap in the active site of BACE1 as revealed by crystal structures and molecular dynamics simulations. *Acta Crystallogr., Sect. D: Biol. Crystallogr.* **2012,** *D68*, 13-25.

48. Banner, D. W.; Gsell, B.; Benz, J.; Bertschinger, J.; Burger, D.; Brack, S.; Cuppuleri, S.; Debulpaep, M.; Gast, A.; Grabulovski, D.; Hennig, M.; Hilpert, H.; Huber, W.; Kuglstatter, A.; Kusznir, E.; Laeremans, T.; Matile, H.; Miscenic, C.; a, Rufer, A.; Schlatter, D.; Staeyert, J.; Stihle, M.; Thoma, R.; Weber, M.; Ruf, A. Mapping the conformational space accessible to BACE2 using surface mutants and co-crystals with Fab-fragments, Fynomers, and Xaperones. *Acta Crystallogr., Sect. D*, in press.

49. Jensen, H. H.; Lyngbye, L.; Jensen, A.; Bols, M. Stereoelectronic substituent effects in polyhydroxylated piperidines and hexahydropyridazines. *Chem.--Eur. J.* **2002,** *8*, 1218-1226.

50. Morgenthaler, M.; Schweizer, E.; Hoffmann-Roder, A.; Benini, F.; Martin, R. E.; Jaeschke, G.; Wagner, B.; Fischer, H.; Bendels, S.; Zimmerli, D.; Schneider, J.; Diederich, F.; Kansy, M.; Muller, K.

Predicting and tuning physicochemical properties in lead optimization: amine basicities. *ChemMedChem* **2007,** *2*, 1100-1115.

51. Woltering, T. Halogen-alkyl-1,3 oxazines as BACE1 and/or BACE2 inhibitors and their preparation. WO2012168164A1, 2012.

52. VAMP (Version 9.0), Accelrys Inc., San Diego, USA (http://www.accelrys.com)

53. Rueeger, H.; Lueoend, R.; Rogel, O.; Rondeau, J.-M.; Mobitz, H.; Machauer, R.; Jacobson, L.; Staufenbiel, M.; Desrayaud, S.; Neumann, U. Discovery of Cyclic Sulfone Hydroxyethylamines as Potent and Selective β-Site APP-Cleaving Enzyme 1 (BACE1) Inhibitors: Structure-Based Design and in Vivo Reduction of Amyloid β-Peptides. *J. Med. Chem.* **2012,** *55*, 3364-3386.

54. Stamford, A. W.; Scott, J. D.; Li, S. W.; Babu, S.; Tadesse, D.; Hunter, R.; Wu, Y.; Misiaszek, J.; Cumming, J. N.; Gilbert, E. J.; Huang, C.; McKittrick, B. A.; Hong, L.; Guo, T.; Zhu, Z.; Strickland, C.; Orth, P.; Voigt, J. H.; Kennedy, M. E.; Chen, X.; Kuvelkar, R.; Hodgson, R.; Hyde, L. A.; Cox, K.; Favreau, L.; Parker, E. M.; Greenlee, W. J. Discovery of an Orally Available, Brain Penetrant BACE1 Inhibitor That Affords Robust CNS Aβ Reduction. *ACS Med. Chem. Lett.* **2012,** *3*, 897-902.

55. Truong, A. P.; Toth, G.; Probst, G. D.; Sealy, J. M.; Bowers, S.; Wone, D. W. G.; Dressen, D.; Hom, R. K.; Konradi, A. W.; Sham, H. L.; Wu, J.; Peterson, B. T.; Ruslim, L.; Bova, M. P.; Kholodenko, D.; Motter, R. N.; Bard, F.; Santiago, P.; Ni, H.; Chian, D.; Soriano, F.; Cole, T.; Brigham, E. F.; Wong, K.; Zmolek, W.; Goldbach, E.; Samant, B.; Chen, L.; Zhang, H.; Nakamura, D. F.; Quinn, K. P.; Yednock, T. A.; Sauer, J.-M. Design of an orally efficacious hydroxyethylamine (HEA) BACE-1 inhibitor in a preclinical animal model. *Bioorg. Med. Chem. Lett.* **2010,** *20*, 6231-6236.

56. Aronov, A. M. Ligand structural aspects of hERG channel blockade. *Curr. Top. Med. Chem. (Sharjah, United Arab Emirates)* **2008,** *8*, 1113-1127.

57. El, M. M.; Haseldonckx, M.; Mackie, C.; Meert, T.; Mercken, M. Method for the determination of the levels of β-amyloid peptide in the CSF sampled from freely moving rats. *J. Pharmacol. Toxicol. Methods* **2005,** *52*, 229-233.

58. Gruninger-Leitch, F.; Schlatter, D.; Kung, E.; Nelbock, P.; Dobeli, H. Substrate and inhibitor profile of BACE (β-secretase) and comparison with other mammalian aspartic proteases. *J. Biol. Chem.* **2002,** *277*, 4687-4693.

59. Martin, R. E.; Mohr, P.; Maerki, H. P.; Guba, W.; Kuratli, C.; Gavelle, O.; Binggeli, A.; Bendels, S.; Alvarez-Sanchez, R.; Alker, A.; Polonchuk, L.; Christ, A. D. Benzoxazole piperidines as selective and potent somatostatin receptor subtype 5 antagonists. *Bioorg. Med. Chem. Lett.* **2009,** *19*, 6106-6113.

60. Kuglstatter, A.; Stahl, M.; Peters, J.-U.; Huber, W.; Stihle, M.; Schlatter, D.; Benz, J.; Ruf, A.; Roth, D.; Enderle, T.; Hennig, M. Tyramine fragment binding to BACE-1. *Bioorg. Med. Chem. Lett.* **2008,** *18*, 1304-1307.

61. Lanz, T. A.; Schachter, J. B. Demonstration of a common artifact in immunosorbent assays of brain extracts: Development of a solid-phase extraction protocol to enable measurement of amyloid-β from wild-type rodent brain. *J. Neurosci. Methods* **2006,** *157*, 71-81.

62. Brockhaus, M.; Grunberg, J.; Rohrig, S.; Loetscher, H.; Wittenburg, N.; Baumeister, R.; Jacobsen, H.; Haass, C. Caspase-mediated cleavage is not required for the activity of presenilins in amyloidogenesis and NOTCH signaling. *NeuroReport* **1998,** *9*, 1481-1486.

Table of Contents Graphic